The Design of Whispering Gallery Mirrors for Soft X-Ray Lasers

by

Tsen-Yu Hung

Submitted to the Department of Electrical Engineering and Computer Science
in Partial Fulfillment of the Requirements for the Degree of
Bachelor of Science in Electrical [Computer] Science and Engineering
at the Massachusetts Institute of Technology
May 1988

Author _____

Department of Electrical Engineering and Computer Science
May 10, 1988

Certified by _____ May 10, 1988

Peter L. Hagelstein, Associate Professor
Thesis Supervisor

Accepted by _____

Leonard A. Gould
Chairman, Department Committee on Undergraduate Theses

THE DESIGN OF WHISPERING GALLERY MIRRORS FOR SOFT X-RAY LASERS

by

Tsen-Yu Hung

Submitted to the Department of Electrical Engineering and Computer Science on May 10, 1988 in partial fulfillment of the requirements for the degree of Bachelor of Science.

Abstract

Whispering Gallery Mirrors are broad band soft x-ray mirrors that have been demonstrated to achieve close to 70% reflectivity for 180 degree turn, or close to 50% reflectivity for 360 degree turn, which is higher performing than other designs, such as the multilayer mirrors. Both the theoretical and experimental aspects of the mirrors are explored in detail.

Literature on the analysis of the electromagnetic field for cylindrical boundary and perfectly conducting and lossy medium is reviewed in detail, from the earliest analysis accomplished by Lord Rayleigh.

Reports on progress made in manipulating the 2D Helmholtz equation for numerical modeling are included. Examinations of both the high frequency limit and the low frequency limit (which correspond physically to x-ray radiation and infrared waveguides, respectively) are described.

Losses of soft x-rays due to scattering is studied by modelling the surface irregularities as Gaussian distribution. Surface smoothness requirements for soft x-rays are described.

Losses due to photoabsorption is studied by examining the materials' Cooper Minimum. The term, Cooper Minimum, is briefly explained. Kramer-Kronig analysis is described here and will be used in the near future to compute the optical constants of promising materials for surface coatings.

A survey of the susceptibility to oxidation, toxicity, malleability, and the Cooper Minimum wavelength of the elements Z = 36 - 94 is included. A selection of materials for whispering gallery mirror to reflect light of 200 angstroms wavelength is chosen and described.

Industries who can polish surfaces on the order of tens of angstroms are described. Issues in constructing the whispering gallery mirrors and their solutions are discussed. Techniques to evaluate surface roughness are examined.

Thesis Supervisor: Prof. Peter L. Hagelstein
Title: Associate Professor of Electrical Engineering and Computer Science

Acknowledgements

I express my deepest appreciations to Prof. Peter Hagelstein. His goeing out of his way to satisfy his students' curiosities impresses me. His intellects are beyond brilliance. He, as a mentor, places equal weights in developing his students in both as a scientist and a human being.

I thank Prof. Hank Smith for his caring supports and suggestions.

I would also like to thank Mary Ellen Butts, our group's secretary, for her support.

TABLE OF CONTENTS

LIST OF FIGURES

I. INTRODUCTION

All materials' reflecting power, at normal incidence, deteriorates rapidly when the incoming light's wavelength becomes less than 400 angstroms. At optical wavelengths ($\approx$ 2000 angstroms), reflectivity close to unity has been achieved. However, for soft x-rays, losses incurred by photoabsorption make it impossible to achieve similar high reflecting power. Only close to 40% of reflectivity has been achieved in the multilayer mirror schemes.[1]. Here, we are proposing a different scheme, the whisper gallery mirrors (See Fig-

ure I.1). Close to 50% has been demonstrated by an experiment conducted by Vinogradov.[2]

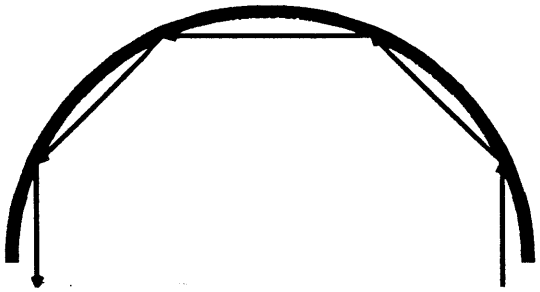

Figure I.1 Whispering Gallery Mirror

The name, "whispering gallery", was first used by Lord Rayleigh to describe the trapping of high frequency fields, in our example, by a concave surface. The incoming light beam, represented by arrows in the figure, hits the mirror at a shallow angle. The beam bounces around the mirror and is turned 180 degrees in the mirror shown.

We, the MIT Short Wavelength Laser Group, are currently designing and building a table-top soft x-ray laser. The major thrust of this thesis' research is to explore and develop optics for the soft x-ray laser. In our experimental design, we wish to see maximum reflectivity at approximately 195 angstroms. The theory and implementation issues discussed in this thesis does not limit itself to that specific wavelength. The specific wavelength is, rather, more often used as an example to demonstrate the principles and results.

To design the mirrors for soft x-rays, we can take either of the two approaches: multilayer mirrors or whispering gallery mirrors. In the multilayer mirrors,[1,3–9] soft x-rays are

shined on the material at normal incidence (Figure I.2). Each layer is $\frac{\lambda}{4}$ thick, so that the optical path of the reflected beam is $\frac{\lambda}{2}$. Those reflected light beam add in phase; and we receive a considerable amount reflected light back.

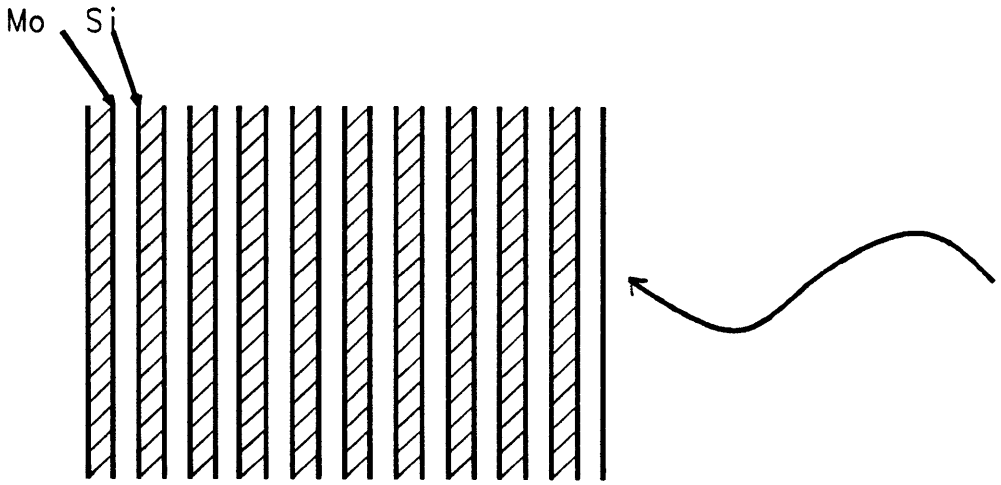

Figure I.2 Multilayer Mirror

Multilayer mirrors are periodic structures of absorbing (Si) and reflecting (Mo) layers.

Some of the highest reflectivities, in the soft x-ray range, that have been demonstrated hover around 40%.[1] Multilayer mirrors have advanced tremendously in the last decade through the use of synthetic layers. However, not everyone has the facilities to build multilayer mirrors with synthetic layers and not everyone can do a precise job in building them. The other major problem associated with multilayer mirrors is that they are extremely wavelength sensitive, i.e., narrow-banded. In Figure I.3, the reflectivity of the

mirror drops from 40% to 20% when the wavelength changes by 3.0%.

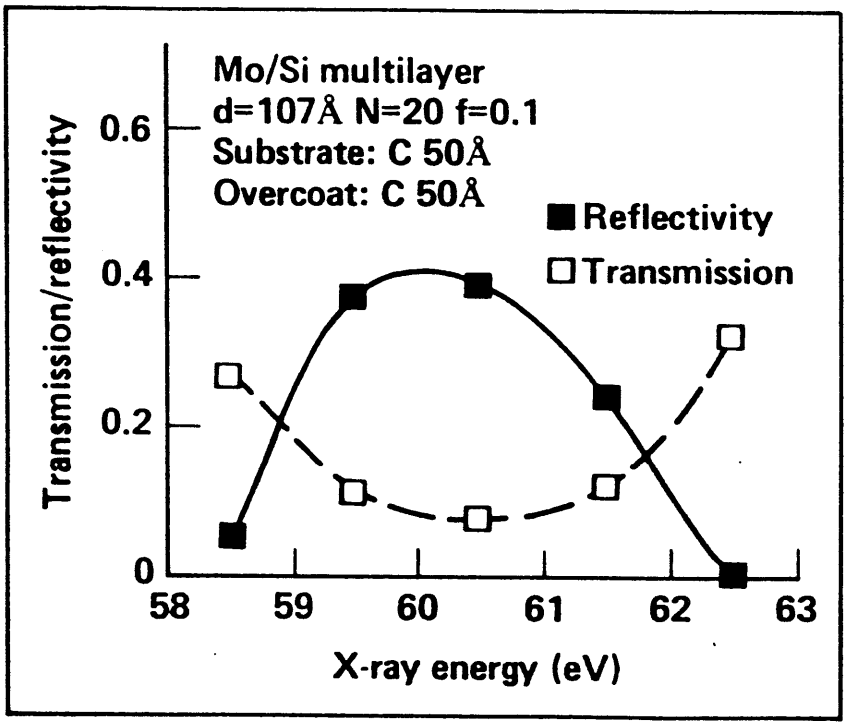

Figure I.3 Transmission/reflectivity vs. X-ray energy plot

The amount of transmission/reflectivity of a multilayer soft x-ray optical structure is plotted against the incoming light's energy. The peak of the mirror's reflectivity occurs for incoming light with a wavelength of 206 angstroms. **(Courtesy of Ceglio N. M.)**

Similarly, in Figure I.4, the reflectivity drops from 60% to 50% when the wavelength changes by 3.4%. In addition, the focusing optics still in its infancy for multilayer mirrors

due to its rigid geometry.

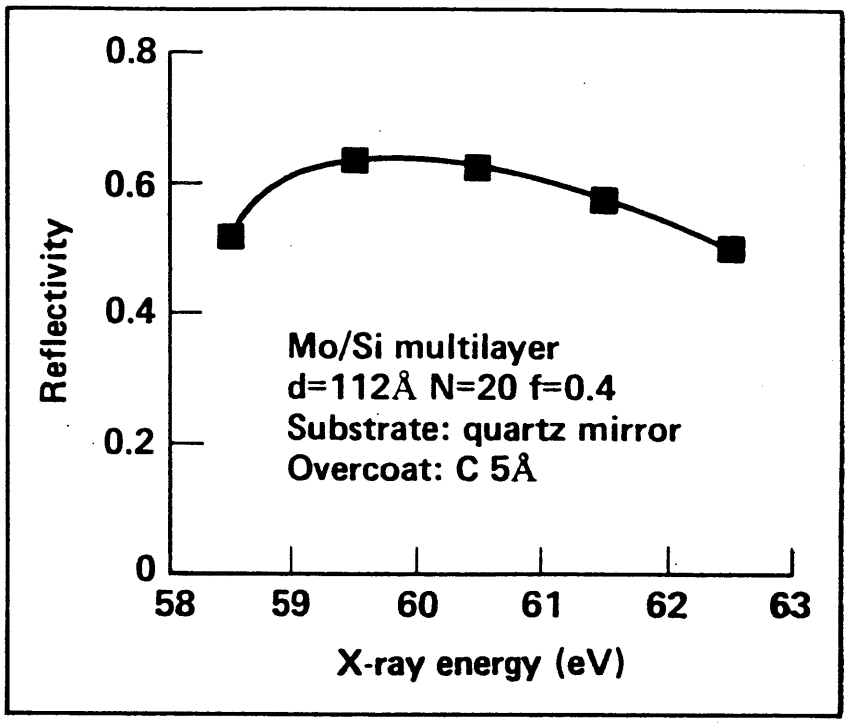

Figure I.4 Reflectivity vs. X-ray energy plot

The reflectivity of a multilayer soft x-ray mirror is plotted against the incoming light's energy. The peak of the mirror's reflectivity occurs for incoming light with a wavelength of 209 angstroms **(Courtesy of Ceglio N. M.)**

Whispering gallery mirrors, on the other hand, are broad band soft x-ray mirrors. Material's *Cooper Minima* , at which the maximum reflectivity can be achieved, occurs at a wider range of wavelengths compared to the narrow, specific wavelength for absorption edges. This property is what makes whispering gallery mirrors broad band and versatile as compared to multilayer mirrors. As we can see in Vinogradov's data (Figure I.5): for Rh,

the reflectivity only drops from 65% to 55% when the incoming light's wavelength changes by 8.3%.

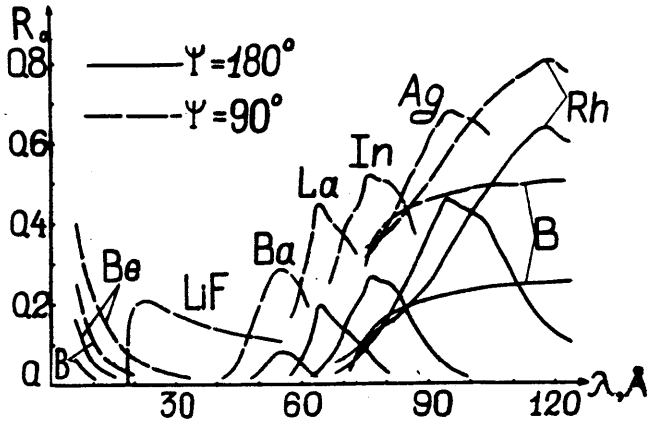

Figure I.5 Vinogradov's Data

Vinogradov plotted the reflectivity of a whispering gallery mirror with 180 degree or 90 degree turn. The reflectivity of mirrors with 180 degree turn is approximately the square of the reflectivity of mirrors with 90 degree turn

The reflectivity decreases gently to 20% only when the incoming light's wavelength changes by as much as 25%.

We will first examine, in Chapter 2, what has been done in the design of the whispering gallery mirrors. Theoretically, the idea has been studied widely for acoustic waves. Lord Rayleigh pioneered the study of whispering gallery modes. Experimentally, on the other hand, it has only been carried out recently for soft x-rays by Vinogradov of P. N. Lebedev of Physics Institute.

The major literature review of the study of whispering gallery modes is extremely mathematical. It can be found in the appendices. Readers who are only interested in getting a flavor of what the "whispering gallery" mirrors are need not skim through this section.

In Chapter 3, both practical and theoretical design issues are discussed. A design on size and the shape of the mirror is discussed in the first section. The size of the glancing angle is determined by the optical constant of the material at their particular Cooper minimum wavelengths. In the third section, we study, from two approaches the effect of perturbations from a perfectly smooth surface on the mirror's reflectivity. The requirement for our implementation is also described. In the last section, the Kramers-Kronig analysis, which will be used to calculate the optical constants of the materials, is described. This section also has a table of all elements that displays Cooper minimum in the wavelength range that we are interested in. Their properties are listed so that we can examine which element should be used over the others.

We would like to write a program to analyze the 2D Helmholtz equation. A progress report is included in here as to how have we been manipulating the Helmholtz equation. The first section examines the high frequency approximation, which, physically correspond to the x-ray mirror design. The second section examine the low frequency approximation, which, physically correspond to the infrared waves. We also present another approach to solve the problem, the gradient method, which is useful for solving heterogeneous boundary conditions.

In Chapter 4, we examine the issues involved in implementing the mirrors. We examined what Perkin-Elmers has done in building the Space X-Ray Telescope. They have achieved a surface smoothness of 15 angstroms on the average. We will discuss what it would take to

build the whispering gallery mirrors locally. The measuring techniques are also discussed for both approaches.

Issues that are yet to be investigated are discussed in Chapter 5. Whispering gallery mirrors places stringent requirements on the quality of the surface. Large companies, such as Perkin-Elmers, have successfuly built the x-ray telescope. However, such procedure has not been commercialized. We have only been able to find one local industry to undertake such a construction.

Cambridge, Mass., May 1988 Judy Hung

II. Present Status of the Whispering Gallery Mirrors

Presently, x-ray optics utilizing the whispering gallery sliding modes have only been built and tested by A. V. Vinogradov at the P. N. Lebedev Physics Institute. Vinogradov have tested whispering gallery mirrors for wavelengths range from 10 to 120 angstroms. For mirror of rotation angle of 180 degrees, he has achieved close to 70% reflectivity (or close to 50% for 360 degrees) for wavelength of 120 angstroms using a Rh coating. The material that coats the mirror is rhodium, Rh. He has also tested other material coatings such as Ag, B, In, La, Ba, LiF, and Be for different wavelengths.

Lord Rayleigh[1] was the first one to study whispering gallery modes in wave propagation. He pioneered the mathematical analysis, such as the high frequency expansion of the Bessel functions, needed to analyze such problems. He solved the problem for both perfectly conducting and lossy boundary. Recent important work includes ones accomplished by: Wasylkiwskyj[3], Ishida & Felsen[4], and others explore further into the problems. The

boundary geometry so far treated are all cylindrical. Bahar[5], in solving wave propagation problems along irregular soil surfaces, formulated mathematical expression studying boundary that is consisted of different radii of curvature. Even though Bahar treated a more general problem, his mathematical expressions are hard to manipulate.

In this section, we will examine briefly what each of them have accomplished in the analysis of whispering gallery modes. Detailed derivations, done by Lord Rayleigh, Wasylkiwskyj, and Bahar, can be found in Appendix A, B, and C, respectively, for interested reader.

After this literature review, we will outline the problem that we are interested in solving: electromagnetic (EM) field on an arbitrarily shaped surface. We will outline the problem at the end of this section. What we have accomplished so far in solving the problem will be found in Chapter 3, Section B.

II.1 LORD RAYLEIGH'S FORMULATION

A whispering gallery mode, a hump of energy as shown in Figure II.1.1,

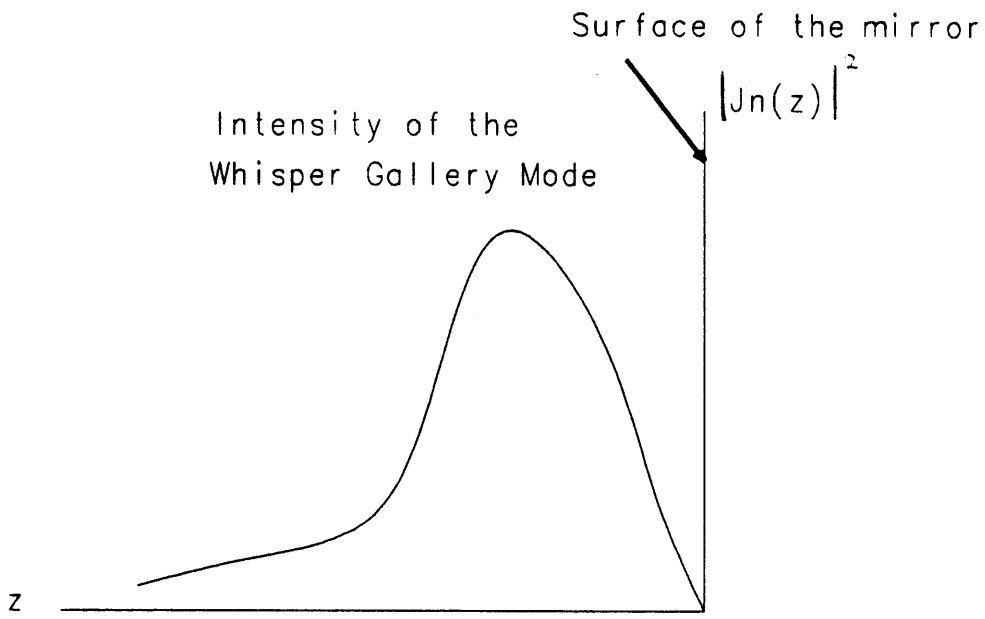

Figure II.1.1

The intensity of a whispering gallery mode is described by the square of a Bessel's function. The closeness of the hump of energy to the surface of the mirror is what made Lord Rayleigh call it a "clinging" wave. is described by Lord Rayleigh as a field that "clings" around a concave surface. Lord Rayleigh pioneered the mathematical description of the trapping of the high frequency fields inside cylindrical surfaces. He first described how high frequency

waves (in his experiment, a bird call) propagate around the dome of St. Paul's cathedral with exceptionally low loss. However, he did not analyze mathematically the phenomenon until 30 years later(in 1910). He first analyzed a perfectly conducting surface.[1] He later treated the problem for a lossy medium.[2] His analysis of high frequency fields paralleled his analysis of the waves traveling on a membrane, a problem that he had already analyzed mathematically in his *Theory of Sound.*[6] Nevertheless, he needed to take the higher order expansion of the Bessel functions, a technique which was only just developing at the time when he published his mathematical analysis. In our application, we use smaller structures to achieve the similiar effect for the much higher frequency x-rays.

A wave which travels around a cylindrical surface can be described in terms of a Bessel function

$$w(r,\theta,t) = AJ_n(kr)\cos(kct - n\theta) \qquad (II.1.1)$$

where w is the displacement of the membrane, which parallels the E field in our analysis and $J_n(kr)$ is the Bessel function. The acoustic wave travels with the velocity c, and $k = 2\pi/\lambda$. The waves oscillate around the cylinder with a discrete number of wavelength.

We will explain why the waves have such dependence. w satisfies the wave equation,

$$\frac{d^2w}{dr^2} + \frac{1}{r}\frac{dw}{dr} + \frac{1}{r^2}\frac{d^2w}{d\theta^2} + k^2w^2 = 0 \qquad (II.1.2)$$

w is harmonic in time and can be expanded into a Fourier series:

$$w(r,\theta,t) = w_m(r)cos[m(\theta + \alpha_m)]e^{ikct} \qquad (II.1.3a)$$

$$\sum_m \left\{ \frac{d^2w_m}{dr^2} + \frac{1}{r}\frac{dw_m}{dr} + (k^2 - \frac{m^2}{r^2})w_m \right\} \cos m(\theta + \alpha_m) = 0 \qquad (II.1.3b)$$

If we multiply this sum by $cos[n(\theta + \alpha_n)]$ and integrate it with respect to θ from 0 to 2π, we obtain,

$$\frac{d^2w_n}{dr^2} + \frac{1}{r}\frac{dw_n}{dr} + (k^2 - \frac{n^2}{r^2})w_n = 0 \qquad (II.1.4)$$

which is Bessel's equation. There exist two distinct solutions to Bessel's equation (a regular and an irregular solution). We will use the regular solution ($J_n(kr)$) because the other solution becomes singular at the origin. The index of this Bessel function n takes on integer values because the waves have to retrace themselves around the cylindrical surface. Therefore, we can express $J_n(kr)$ in the following form:

$$J_n(kr) = \frac{1}{\pi}\int_0^{\pi} \cos(n\sin\psi - kr)d\psi \qquad (II.1.5)$$

The boundary condition for a perfectly conducting surface is

$$J_n(kR) = 0 \qquad (II.1.6)$$

The "whispering gallery" modes correspond to the first zero that occurs away from the surface.

For a lossy medium, the approach for solving for the transmission of the displacement on the membrane w, which parallels the E field in our analysis can be shown to be (Appendix A)

$$Transmission = 1 - \frac{2\pi\mu\sigma}{n\rho}e^{\frac{-2n(\beta-\tanh\beta)}{\sinh\beta}} \qquad (II.1.7)$$

where μ is the ratio of the refractive index of inside with respect to the refractive index of the boundary (outside); σ and ρ are the densities inside and outside the surface respectively; and β obeys the relation: $z = n\cosh\beta$. If n is big, i.e., the frequency is high the damping is not significant. Moreover, the less curved the surface is, the smaller μ needs to be.

Therefore, for a lossy medium, the whispering gallery effect may still persist given that the frequency of the waves is high enough.

II.2 WASYLKIWSKYJ'S FORMULATION

Green's functions are kernel functions used to describe electromagnetic radiations. Its mathematical representation provides a pleasing and accesible way to describe the EM fields. Wasylkiwskyj analyzed the high frequency fields on a perfectly conducting surface excited by a line source using Green's functions.[3] He pointed out that to analyze the fields that are excited by a line source we can, as a first approach, use ray optics. We shall collect the field solutions for rays that have been reflected one time, two times, $\cdots$. It is unlikely, however, that this infinite series will provide any numerical insights.

Another way to sum over all the contributions is to use the whispering gallery modes to collect rays that have the same angle of incidence. However, there is only a finite number of such whispering gallery modes, and they are not sufficient enough to describe all the rays emitted from a singular source. The remaining rays constitute a spectral integral which we shall derive shortly.

Wasylkiwkyj used a perfect absorber to enclose the cylindrical surface to absorb any rays that might have been reflected from the plane. The absorber generates some spurious waves. This spurious contribution is small and can be identified.

Through mathematical manipulations, Wasylkiwkyj transformed the Green's function into a ray optics and/or whispering gallery mode representation of the fields. He identified the accuracy for each representation. Therefore, as developed in a later work by Ishihara

and Felsen, it might be necessary to use a combination of such representations to describe the fields.

1. The Whispering Gallery Modes and the Continuous Spectrum Integral Representation

The Green's function's angular dependence assumes the form:

$$g_\phi(\phi|\phi_0;\nu) = \frac{\exp(i\nu|\phi-\phi_0|)}{-2i\nu} \qquad (II.2.1)$$

where ϕ_0 denotes the angle at which the source point is located and ν is the propagation constant of the waves.

The Green's function can be expanded into a set of eigenfunctions:

$$G(\bar{r}|\bar{r}_0) = \sum_\nu g_\phi(\phi|\phi_0;\nu)\psi_\nu(r)\psi_\nu(r_0) \qquad (II.2.2)$$

(II.2.2) satisfies the wave equation for a cylindrical surface:

$$\left(\frac{1}{r}\frac{\partial}{\partial r}r\frac{\partial}{\partial r} + \frac{1}{r^2}\frac{\partial^2}{\partial\phi^2} + k^2\right) G(\bar{r}|\bar{r}_0) = -\frac{\delta(r-r_0)\delta(\phi-\phi_0)}{r_0} \qquad (II.2.3)$$

The perfectly reflecting surface has the boundary condition,

$$\frac{\partial}{\partial r}G(\bar{r}|\bar{r}_0)\Big|_{r=a} = 0 \qquad (II.2.4)$$

with a as the radius of the cylinder.

We obtain, for the Green's function:

$$G(a,\phi,\phi_0) = \frac{i}{ka}\sum_{n=1}^{N}\frac{e^{ika|\phi-\phi_0|}\sin w_n}{(\pi/2-w_n)\cos w_n} +$$

$$\frac{1}{\pi}\int_0^\infty dv e^{-ka|\phi-\phi_0|\sinh hv} + 0\left(\frac{1}{ka}\right) \qquad (II.2.5)$$

where the first term is the whispering gallery modes and the second term the continuous spectrum integral. The last term is the spurious effect generated by the absorbing boundary condition. Detailed derivation can be found in Appendix B for interested readers.

2. Geometrical Ray Representation

In the geometrical ray representation, we try to represent the Green's function as consisted of rays that bounces off the cylindrical surface 1, 2, $\cdots$, l times. To establish a geometrical ray representation of the fields, we use a Fourier transform representation of the Green's function:

$$G(\bar{r}|\bar{r}_0) = \frac{1}{2\pi}\int_{-\infty}^{\infty} e^{i\nu|\phi-\phi_0|} g_r(r|r_0;\nu)d\nu \qquad (II.2.6)$$

which we take the high frequency expansion and is shown in Appendix B to be :

$$G(a,\phi,\phi_0) \sim \sum_{l-1}^{\infty}(-1)^l e^{i(\pi/2)(l+1)l} \qquad (II.2.7)$$

summing over all rays.

3. Geometric Optics and the Whispering Gallery Modes Representation

Wasylkiwskyj tries to compensate the imperfection in each formulation by using a combination of the the geometric optics and the whispering gallery modes representation, he arrives at the result:

$$\begin{aligned} G(a,\phi,\phi_0) \;\sim\; & \sum_{l=1}^{L}(-1)^l e^{i(\pi/2)(l+1)} F_l(a,\phi,\phi_0) \\ & + \frac{1}{2}(-1)^{L+1} e^{i(\pi/2)(L+2)} F_{L+1}(a,\phi,\phi_0) \\ & + \frac{i}{ka}\sum_{n=1}^{M} \frac{e^{ika\left|\phi-\phi_0\right|\sin Wn}}{(\pi/2-W_n)\cos Wn} \end{aligned} \qquad (II.2.8)$$

where the first term is the geometric rays and the last term the whispering gallery modes. The second corrects for the field that is not represented by either of the two representation.

II.3 ISHIHARA and FELSEN'S FORMULATION

Ishihara and Felsen reconstructed each of Wasylkiwskyj's formulation of the high frequency fields on a perfectly conducting cylindrical surface that is excited by a line source. They verified the accuracy of each formulation numerically and developed a representation to explain the fields that are close to the source point.[4]

All formulations except for the whispering gallery modes plus the canonical integral representation fail to explain what happens to the field when the observation point is close to the source point. The ray optics representation fails miserably when the observation point gets close to the source point. This is so because when we try to get close to the source point, numerous caustics are formed. Even if we try to scrape up the contributions from those caustics by collecting them in an integral expression, the integrand is shown to diverge. The whispering gallery modes and the ray optics representation, on the other hand, do not explain what is on the surface field either. The ray optics terms in this representation, again, diverge when the observation point gets close to the source point. We shall resort to the integral expression of the field,

$$G(\bar{r}|\bar{r}_0) = \frac{1}{i(\pi ka)^2}\int_c \frac{e^{i\nu|\phi-\phi'|}}{H_\nu'^{(2)}(ka)J_\nu'(ka)}d\nu \qquad (II.3.1)$$

After we take the respective contour integral and plug in the appropriate Wronskian

relation, (II.3.1) is shown by Ishihara and Felsen to reduce down to

$$G \sim -\frac{e^{iks}}{2\pi ka}\left(\frac{ka}{2}\right)^{2/3}\int_{-\infty-i\delta}^{+\infty-i\delta} e^{i\Upsilon t}\frac{Ai(t)}{\dot{A}i(t)}dt \qquad (II.3.2)$$

where

$$\Upsilon = \left(\frac{ka}{2}\right)^{1/3}\frac{s}{a} \qquad (II.3.2a)$$

and

$$s = a\,|\phi - \phi'| \qquad (II.3.2b)$$

Part of the integrand in (II.3.2) can be shown to be expanded into

$$-\frac{Ai(t)}{\dot{A}i(t)} \sim \sum_{j=0}^{10}\frac{aj}{t^{(1+3j)/2}} + 0(t^{-34/2}), -\pi < argt < 0 \qquad (II.3.3)$$

By Laplace's inversion, (II.3.3) can be expanded into the terms

$$G \sim \frac{i}{2}H_0^{(1)}(ks)\left\{\sum_{j=0}^{10} b_j \Upsilon^{(3/2)j} + 0(\Upsilon^{33/2})\right\} \qquad (II.3.4)$$

The coefficients in the series are given:

$b_0 = 1$

$b_1 = \sqrt{\pi}e^{i\pi/4}/4$

$b_2 = -7i/60$

$b_3 = -7\sqrt{\pi}e^{i\pi/4}/512$

$b_4 = -.4398134 \times 10^{-2}$

$b_5 = -.4109687 \times 10^{-3}\sqrt{\pi}e^{i\pi/4}$

$b_6 = .1122861 \times 10^{-3}i$

$b_7 = .9182121 \times 10^{-5}\sqrt{\pi}e^{i\pi/4}$

$b_8 = .2093046 \times 10^{-5}$

$b_9 = .1637812 \times 10^{-6}\sqrt{\pi}e^{i\pi/4}$

$b_{10} = -.3633427 \times 10^{-7} i$

$iH_0^{(1)}(ka)/2$ is the Green's function for a perfectly conducting plane.

To analyze the case in which the surface changes from concave to convex while the distance of the convex surface remains the same, we let a change continuously from 0 to 2π.

The whispering gallery mode and continuous spectrum representation gives accurate results except for low ka values, where the whispering gallery eigenfunctions are difficult to be evaluated. In the near field, values are (as previously pointed out by Wasylkiwskyj) dominated by the Neumann's function and the whispering gallery modes.

The whispering gallery mode and canonical integral representation, on the other hand, serves as a good reference for low ka values for the near field calculation. It does not exhibit the whispering gallery mode calculation problem as in the previous representation. The combination of rays and whispering gallery modes, as calculated by Ishihara, provides a good approximation for length within the inequality. For observation points very far away, we have to include a large number of whispering gallery modes. Therefore, the representation becomes hard to calculate.

II.4 BAHAR'S FORMULATION

E. Bahar analyzed the high frequency field on a surface that is of both varying impedance and curvature.[5] This is a more general approach than the one undertaken by Ishihara, Felsen, and Wasylkiwskyj. However, Bahar did not generate numerical results.

Bahar describes a surface of arbitrary curvature and variable impedance by x, y, and z.

The coordinates are defined in the following way: Surfaces on which x are constant are normal to our surface; surfaces on which y are constant enclose the surface ($y > 0$, when y is outside our surface); surfaces on which z are constant are normal to the axis of the cylinder.

The x, y, z coordinates are related to the cylindrical coordinates in the following Jacobians:

$$J_T^{-1} = \begin{vmatrix} \frac{\partial r}{\partial x} & \frac{\partial r}{\partial y} \\ \frac{\partial \phi}{\partial x} & \frac{\partial \phi}{\partial y} \end{vmatrix} = \begin{vmatrix} \frac{dR}{dx} & 1 \\ \frac{1}{R} & 0 \end{vmatrix} \qquad (II.4.1a)$$

$$J_T = \begin{vmatrix} \frac{\partial x}{\partial r} & \frac{\partial x}{\partial \phi} \\ \frac{\partial y}{\partial r} & \frac{\partial y}{\partial \phi} \end{vmatrix} = \begin{vmatrix} 0 & R \\ 1 & -\frac{RdR}{dx} \end{vmatrix} \qquad (II.4.1b)$$

The Maxwell's equations in cylindrical coordinates can be made to depend on x and r while eliminating the ϕ dependent component of the magnetic field. We obtain:

$$-\frac{\partial E_z}{\partial x} = i\omega\mu\frac{r}{R}H_r \qquad (II.4.2a)$$

$$-\frac{\partial H_r}{\partial x} = i\omega\epsilon\left[\frac{r}{R}E_z + \frac{1}{k^2}\frac{\partial}{\partial r}\left(\frac{r}{R}\frac{\partial E_z}{\partial r}\right)\right] + \frac{r}{R}J_z \qquad (II.4.2b)$$

where $k = \omega(\mu\epsilon)^{1/2}$ and $J_z = \frac{I\delta(r-r_0)\delta(x-x_0)}{R}$.

For the cylindrical case, where $r = R$, E_z satisfies the following scalar wave equation:

$$\nabla^2 E_z = \frac{1}{r}\frac{\partial}{\partial r}(r\frac{\partial E_z}{\partial r}) + \frac{1}{r^2}\frac{\partial^2 E_z}{\partial \phi^2} + k^2 E_z = i\omega\mu J_z \qquad (II.4.3)$$

E_z can be expanded into the following eigenfunction expressions for zero impedance.

$$E_z(\xi,\phi) = -\frac{\omega\mu\pi I}{4}\sum H_{\nu_n}^{(2)}(\xi_0)H_{\nu_n}^{(2)}(\xi)\times \left(\frac{H_\nu^{(1)}(\xi_R)}{\frac{\partial H_\nu^{(2)}(\xi_R)}{\partial\nu}}\right)_{\nu_n}\frac{\cos\nu_n(\phi-\phi_0-\pi)}{\sin\nu_n\pi} \qquad (II.4.4)$$

where $H_{\nu_n}^{(1,2)}(\xi)$ are the Hankel functions of the first and second kind and that ξ and ξ_R denote the number of waves in the specified radius.

The electromagnetic fields satifies the impedance boundary condition at $r = R$,

$$\frac{\partial E_z}{\partial(kr)} = \frac{i\eta E_z}{Z_s} \qquad (II.4.5)$$

where η is the intrinsic impedance of the medium.

Each order ν_n of the basis functions satisfy the equation

$$H_{\nu_n}^{(2)'}(\xi_R) - \frac{i\eta}{Z_s}H_{\nu_n}^{(2)}(\xi_R) = 0 (II.4.6)$$

We can write the azimuthal dependence of (II.4.4) as a superposition of the forward traveling and backward traveling waves:

$$E_z(\xi, x) \equiv \sum_n [a_n(x) + b_n(x)] \frac{H^{(2)}_{\nu_n}(\xi)}{N_n} \qquad (II.4.7)$$

We can express the magnetic fields in a similar way:

$$H_r(\xi, x) \equiv \sum_{n=1}^{\infty} [a_n(x) - b_n(x)] \frac{Y_n(\xi) H^{(2)}_{\nu_n}(\xi)}{N_n} \qquad (II.4.8)$$

The forward traveling waves, as noted before by Lord Rayleigh and others, constitutes not only the direct wave propagating in the positive x direction but also the whispering gallery waves which propagate around the cylinder p times (p is an integer).

After a number of manipulations, we obtain for the amplitudes of the traveling waves:

$$a_n(x) = -\int_0^x \frac{dT_{n_0}}{du} a_0(u) \times exp\left[-\int_u^x \left(\frac{dT_{nn}}{dv}\right) + i\left(\frac{\nu_n}{R}\right) dv\right] du \qquad (II.4.9)$$

$$b_n(x) = -\int_x^{\infty} \frac{dT_{n_0}}{du} a_0(u) \times exp\left[-\int_u^x \left(\frac{dT_{nn}}{dv}\right) - i\left(\frac{\nu_n}{R}\right) dv\right] du \qquad (II.4.10)$$

II.5 WHERE DO WE GO FROM HERE

Using mathematical tools, such as the contour integral, WKB method, and asymptotic expansion of the Hankel functions to obtain the Green's function, Lord Rayleigh, Wasylkiwskyj, Ishihara and Felsen, and Bahar have exhausted the development of the Green's function for a cylindrical surface in the high frequency limit. We now outline the approach that we propose to take in solving this problem.

To determine the electromagnetic field in the region of an arbitrary shaped surface containing a high frequency source, we need to use the Huygen's principle. Given that we know the field or its normal derivative everywhere on a closed surface, the Huygen's principle tells us what the field is everywhere inside the surface. We shall rederive it in Appendix A.

The following technique will be used to apply Huygen's principle: we divide the surface into small finite elements (Fig. 1). The field on one finite surface element can be found by summing over the contributions from all other finite element surface fields weighted by a Green's function. The source surface element has an additional source term. If we let E denote either the field itself or its normal derivative, then

$$\mathbf{E}_i = \sum_{\substack{j \\ i \neq j}} \mathbf{G}_{ij}\mathbf{E}_j \qquad i = 2,3,4,\cdots,n$$

$$j = 1,2,3,\cdots,n \qquad (II.5.1a)$$

$$\mathbf{E}_1 = \sum_{\substack{j \\ j \neq 1}} \mathbf{G}_{1j}\mathbf{E}_j + S \qquad j = 2, 3, \cdots, n \qquad (II.5.1b)$$

where $\mathbf{G}_{ij}$ is a Green's function that associates surface i to surface j and S is the source term.

If we know what the Green's functions are, we can solve for the E fields on the surface by solving (II.5.1) self-consistently. However, each finite surface element is large compared to the wavelength of the field.

Recently, we have found literature from Check Lee of Prof. J. A. Kong's group that analyzes the problem of the arbitrarily shaped surface. Check Lee is also working on this problem. The approaches taken by Check Lee and authors of the literature are slightly different than the one we have just described.

The Huygen's principle is derived in Appendix A to establish the theoretical basis of our analysis. We also derive the eigenfunction expansion of the Green's function (Appendix B) because we need this tool to study a light source composed of more than one mode. We shall explore the solution for the Green's function for an arbitrarily shaped surface further in Chapter 3.

III.A.1 The Size and the Shape of the Whispering Gallery Mirrors

It can be shown that the whispering gallery modes are insensitive to the size of the mirrors to the first order. In other words, the reflectance of the whispering gallery mirrors does not depend on the size of the mirror. The geometry of the inner surface, (See photograph of the mirror) determines the number of focal points (See Figure III.A.1) If we wish the

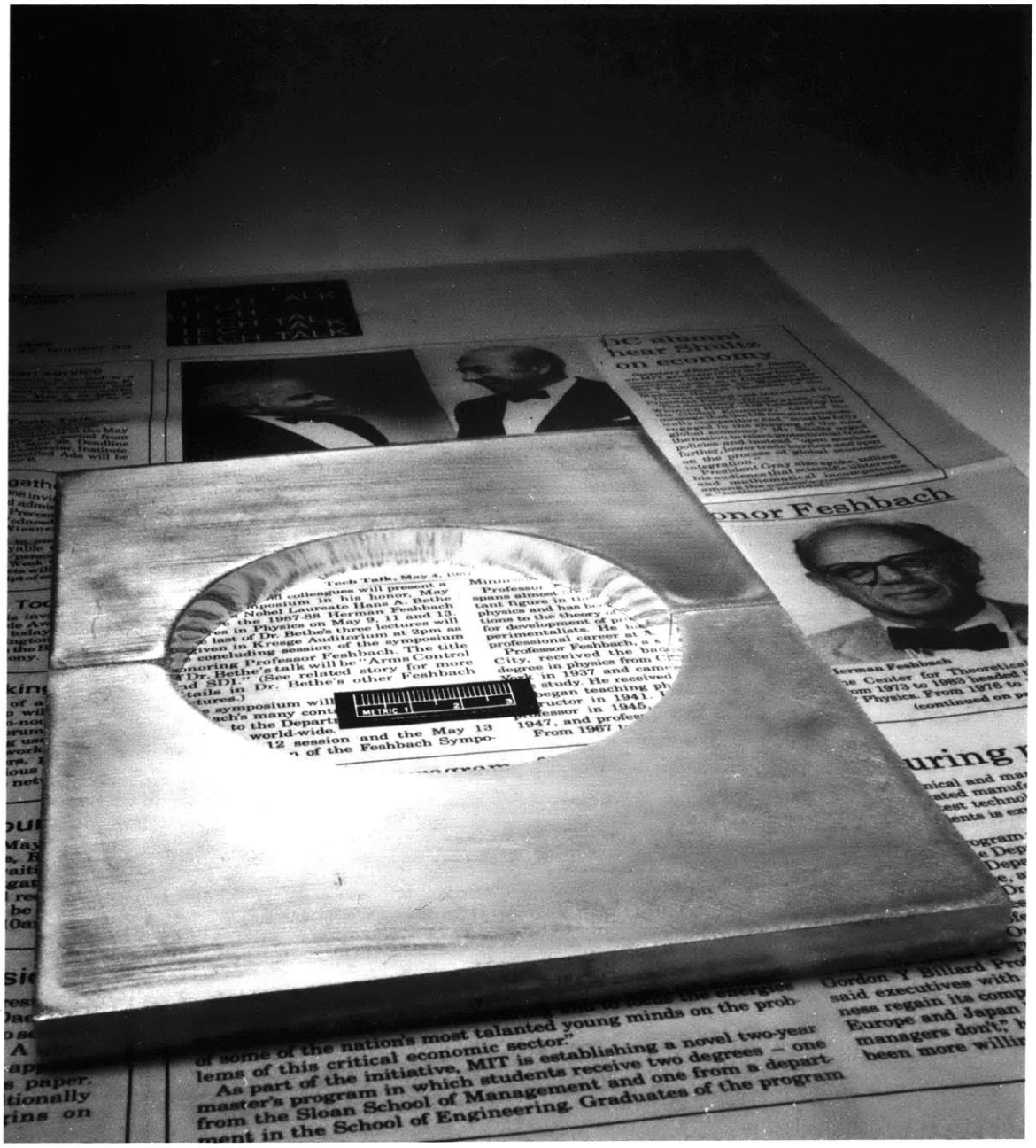
TECH TALK
TECH TALK
TECH TALK
TECH TALK
Tech Talk, May 4, 1988
METRIC 1
2
3
Feshbach
of some of the nation's most talanted young minds on the prob-
lems of this critical economic sector."
As part of the initiative, MIT is establishing a novel two-year
master's program in which students receive two degrees — one
from the Sloan School of Management and one from a depart-
ment in the School of Engineering. Graduates of the program

light beam to focus only at the endpoints of a 360 degree turn mirror, we use elliptical

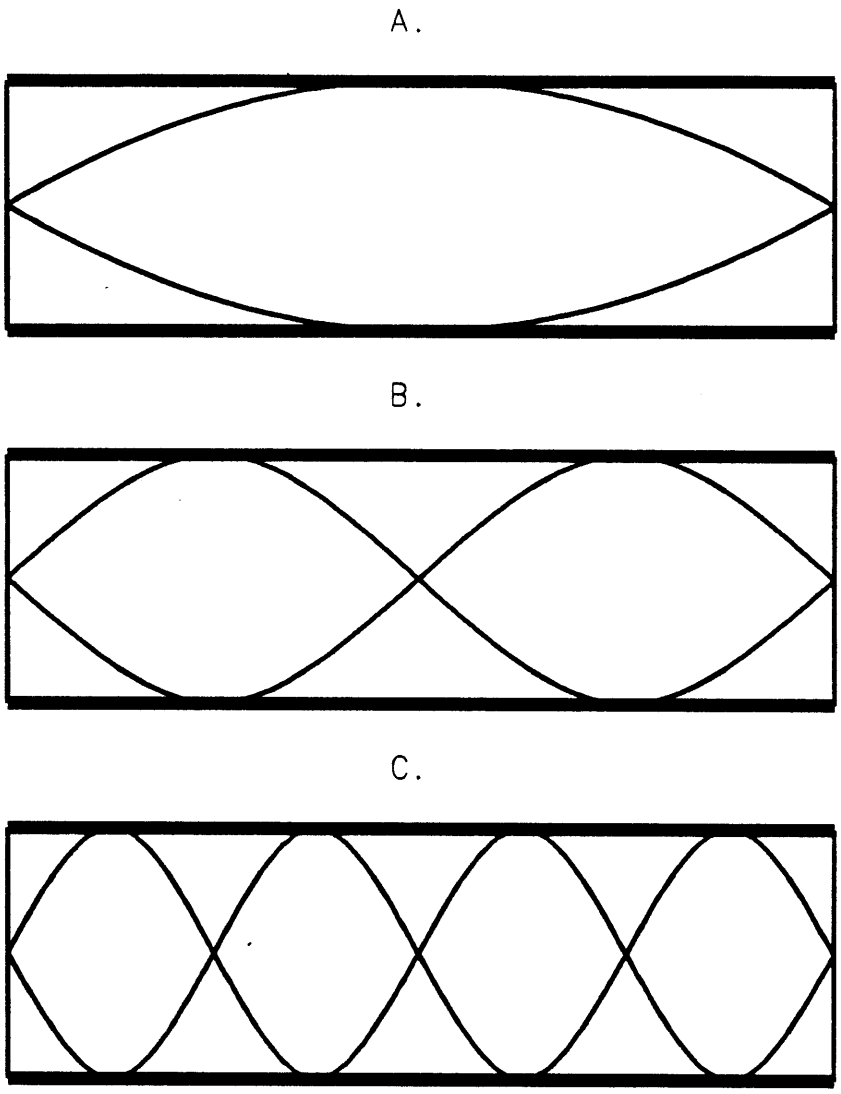

Figure III.A.1 Whispering Gallery Mirror's Focusing Optics

Focusing optics of the whispering gallery mirrors is determined by the geometry of the inside surface. The inside surface of a 360 degree mirror is shown in the figure. A. Elliptic : the focus occurs at the two endpoints; B. Spherical : the focii occur in the center and the the endpoints; C. Toroidal : the number of focii is determined by the toroid's radius of curvature.

surface (A in Figure III.A.1). Spherical surfaces can focus at two points (B in Figure III.A.1). Three or more focal points will require the inner surface geometry be toroidal, with different curvature of radii.

Since the reflectivity of the whispering gallery mirror is independent of the size of the mirror, we can vary the size of the mirror to accomodate the light pulsed that comes in. The size is designed to be at 10 cm diameter to fit the envelope of 15 pulses that comes in. The pulse is 30 nanosecond in duration.

III.A.2 Glancing Angles

In the x-ray regime, all materials' indices of refraction differ little from unity, that is, $n = 1 - \delta$, where δ is a small number[1]. In other words, for a beam of x-ray, the vacuum, whose index of refraction is unity, is optically denser than any material

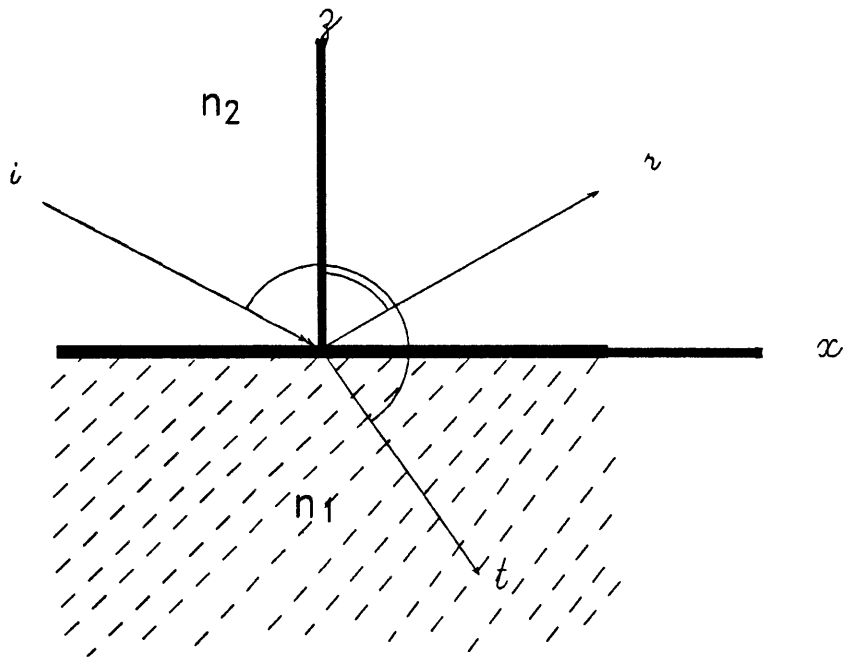

Figure III.A.2.1 Light beam at an interface

Incoming beam, i, coming at an angle θ_i from material with index of refraction n_2, hits a material with index of refraction n_1. Part of the beam is reflected and the other part transmitted.

that constitutes a whispering gallery mirror. Therefore, there exists an angle at which

considerable amount of reflection of x-ray will occur. Because n differs little from unity, this critical angle is extremely small. Those small angles have been referred as grazing incidence angles or glancing angles[2-9].

The light rays in Figure III.A.2.1 obeys the Snell's law which states that the sine of the transmitted angle of the light ray is[10] proportional to the sine of the incident angle of the light ray by a proportion of the refractive indices of the two materials:

$$sin\theta_t = \frac{n_1}{n_2} sin\theta_i \qquad (III.A.1)$$

As stated above, all materials indices of refraction becomes less than unity in the x-ray regime. Therefore, there exist a critical angle θ_c at which the transmitted angle θ_t becomes parallel to the interface and the power of the light ray transmitted become an exponential decay,

$$\theta_c = sin^{-1} \frac{n_1}{n_2} \qquad (III.A.2)$$

In the x-ray regime, the ratio $\frac{n_1}{n_2}$ is very close to 1. The critical angle, θ_c, becomes closer and closer to 90 degrees. The incident ray is grazing the surface of the mirror.

If the index of refraction is complex, so that

$$k = k_r - k_i \qquad (III.A.3)$$

the field attenuate exponentially into the material.

$$E = E_0 e^{-k_i z} \qquad (III.A.4)$$

where z is the depth of the material. Penetration depth of the material is defined to be

$$d_p = \frac{1}{k_i} \qquad (III.A.5)$$

where the field has become $\frac{1}{e}$ of its original values. If the incoming light beam is 200 angstroms, copper's index of refraction is .96 + i.10. Its skin depth would be 10 angstroms. For nickel, the index of refraction for the same wavelength is .98 + i.09. Its skin depth would be 11.1 angstroms. For silver, its index of refraction is .88 + i.21 which leads to a skin depth of 4.76 angstroms.

III.A.1 The size of the glancing angles and beam height

Let us assume that the material has its real part of the refractive index .999, its critical angle is 2.6 degrees, the height of the beam for a mirror with the radius R, is equal to, (by simple geometry) $R[1 - sin\theta_c]$. If the radius is 5 cm, the beam height would be $\approx 51\mu$.

III.A.2 Absorption of soft x-ray in air and one-bounce experiments

It is necessary to work in a vacuum chamber for soft x-ray experiments, because x-rays' penetration depth of an impure environment is very shallow.

In experiments, physicists have dealt extensively with one-bounce experiments to obtain the optical property of the materials[11-14]. Multiple-bounces, as required by the whispering gallery mirrors, have only been carried out extensively by Vinogradov.

III.A.3 Theoretical problems associated with glancing angles

Glancing angles treat the "particle-like" picture of the x-rays. If we work with the particle model, the picture is follows: on each bounce, there is some loss associated with it, the total reflectance of the mirror is consequently dependent on how many bounces there is, and thus dependent on the mirror's size. We can calculate how many bounces that the light particle coming in at an angle θ and turned by a mirror of angle ξ. Each bounce of the particle encompass twice the incidence angle. Therefore, by simple geometry, we can see that the light beam make approximately $\frac{\xi}{\theta}$ bounces. If the incoming beam is .54 degree

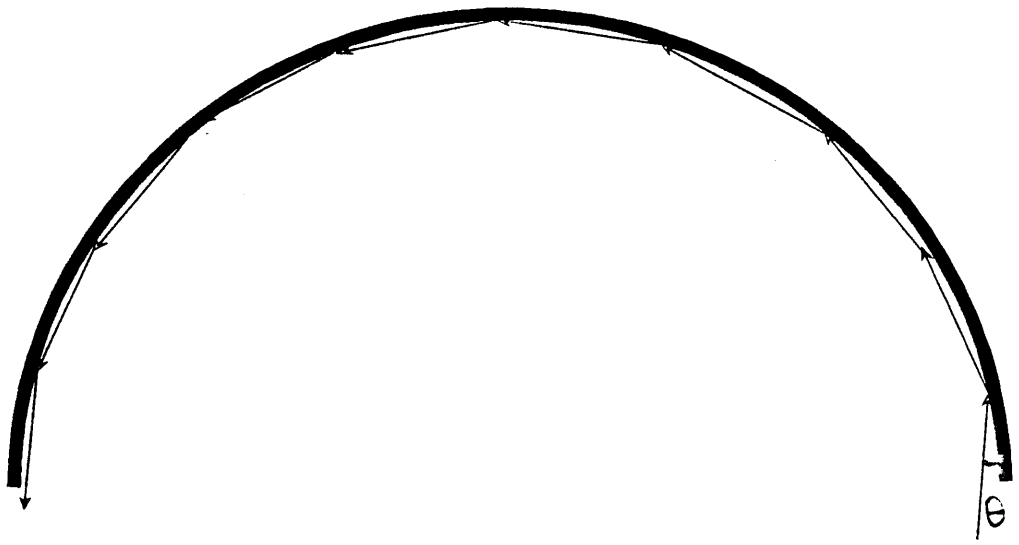

Figure III.A.2.2 Sliding Angle Graph

The incoming light beam, denoted by the arrows in the figure, comes in at a shallow angle θ.

and that the light beam is turned by 180 degrees. The beam would have bounced off the mirror approximately 100 times. Suppose the reflectance of each bounce is 99.7%. The intensity of the beam turned by this 180 deg mirror is approximately 74% of the incoming beam.

III.A.3 Perturbation Analysis of Surface Roughness of the Whispering Gallery Mirrors

It is imperative to consider the effect of the irregularities that are left on the surface have on the reflectivity of the whispering gallery mirrors because they exist inherently in any polished (or superpolished, for that matter) surface.

We can model the imperfect surface as a perfectly smooth surface that has a Gaussian distribution of irregularities with a correlation radius, α and a height, ς.

It is shown by Vinogradov by solving the solving a two dimensional Helmholtz equation adding the surface irregularities as perturbation terms, that the reflectivity of a bent surface mirror is [1]

$$\left|R'\right|^2 = |R|^2 - \delta|R|^2 = |R|^2 \left[1 - 4k^2\varsigma^2\epsilon_1^{\frac{1}{2}}\theta^2\Phi(\mu)\right] \qquad (III.A.3.1)$$

where R is the reflectivity of the bent surface mirror, ϵ_1 is the permittivity of the mirror, θ is the angle of incidence, and k is the wavenumber. μ is a measure of the size of the incidence angle. α is incorporated in the expression μ. It is equal to:

$$\mu = \frac{\alpha k \epsilon_1^{\frac{1}{2}}}{4}\theta^2$$

The expression $\Phi(\mu)$ can be evaluated for two limits: either $\mu \gg 1$ or $\mu \ll 1$ [1]

$$\Phi(\mu) = \frac{\mu J(\mu)}{\pi^{\frac{1}{2}}}$$

$$= 1 - \frac{1}{16\mu^2} + \cdots, \mu \gg 1$$

$$= \frac{1}{2\sqrt{\pi\mu}} \left[\Gamma\left(\frac{3}{4}\right) + \frac{\mu}{2}\Gamma\left(\frac{1}{4}\right) + \cdots \right], \mu \ll 1$$

(*III.A.3.2*)

If the incidence angle is extremely small, as in the case of x rays, Eq. (III.A.3.1) reduces to:

$$\left|R'\right|^2 = |R|^2 \left[1 - \frac{4\epsilon_1^{\frac{3}{4}} \Gamma\left(\frac{3}{4}\right)}{\pi^{\frac{1}{2}}} \frac{(k\varsigma)^2}{(ka)^{\frac{1}{2}}} \right] \qquad (III.A.3.3)$$

For whispering gallery mirrors, we can represent the propagation of the x ray beam as a series of reflections off the mirrors. Consequently,

$$|R(\theta,\phi)|^2 = |R(\theta)|^{\frac{\phi}{\theta}} \qquad (III.A.3.4)$$

There are a large number of reflections. In such limit, Eq. (III.A.3.3) can be shown to transformed to the following expression,

$$|R(\theta,\phi)|^2 = exp\left[-\frac{\phi}{2\theta}\left(1 - |R|^2\right) \right] exp\left[-4\phi \left(\frac{k^3\varsigma^4}{\alpha} \right)^{\frac{1}{2}} \mu^{\frac{1}{2}} \Phi(\mu) \right] \qquad (III.A.3.5)$$

For grazing incidence angle, where $a \approx 0$, the surface is considered smooth if the following condition is satisfied:

$$k^3\varsigma^4 \leq \frac{\alpha}{4\phi} \qquad (III.A.3.6)$$

Since our wavelength is larger compared to correlation radius, we can choose smaller correlation radius, say greater or equal to 1 μ. For incoming light with a wavelength of

200 angstroms hitting a surface with correlation radius of 2 μ, the irregularities' height should be less than 100 angstroms.

Let us calculate the loss of reflectivity due to scattering, which is described by the second exponential term in Eq. (III.A.3.4), for the example just mentioned. There is also losses due to photoabsorption. Let us consider for a mirror that rotate the incoming light beam 180 degrees. If the height of the irregularities is 100 angstroms, as we can see in FigureIII.A.3.1, the loss due to scattering is 82%. Let us assume that loss due to absorption is 30%. The mirror's reflectivity would be 5.4%. If the height reduces by a half to 50 angstroms, the loss due to scattering will have decreased appreciably to 34.8%; the mirror's reflectivity would be $65.2\% \times 30.0\% = 19.5\%$. The scattering becomes closer negligible, when the height reduces to 10 angstroms. The surface's scattering losses are

sensitive to microirregularities with the height between 10 and 100 angstroms.

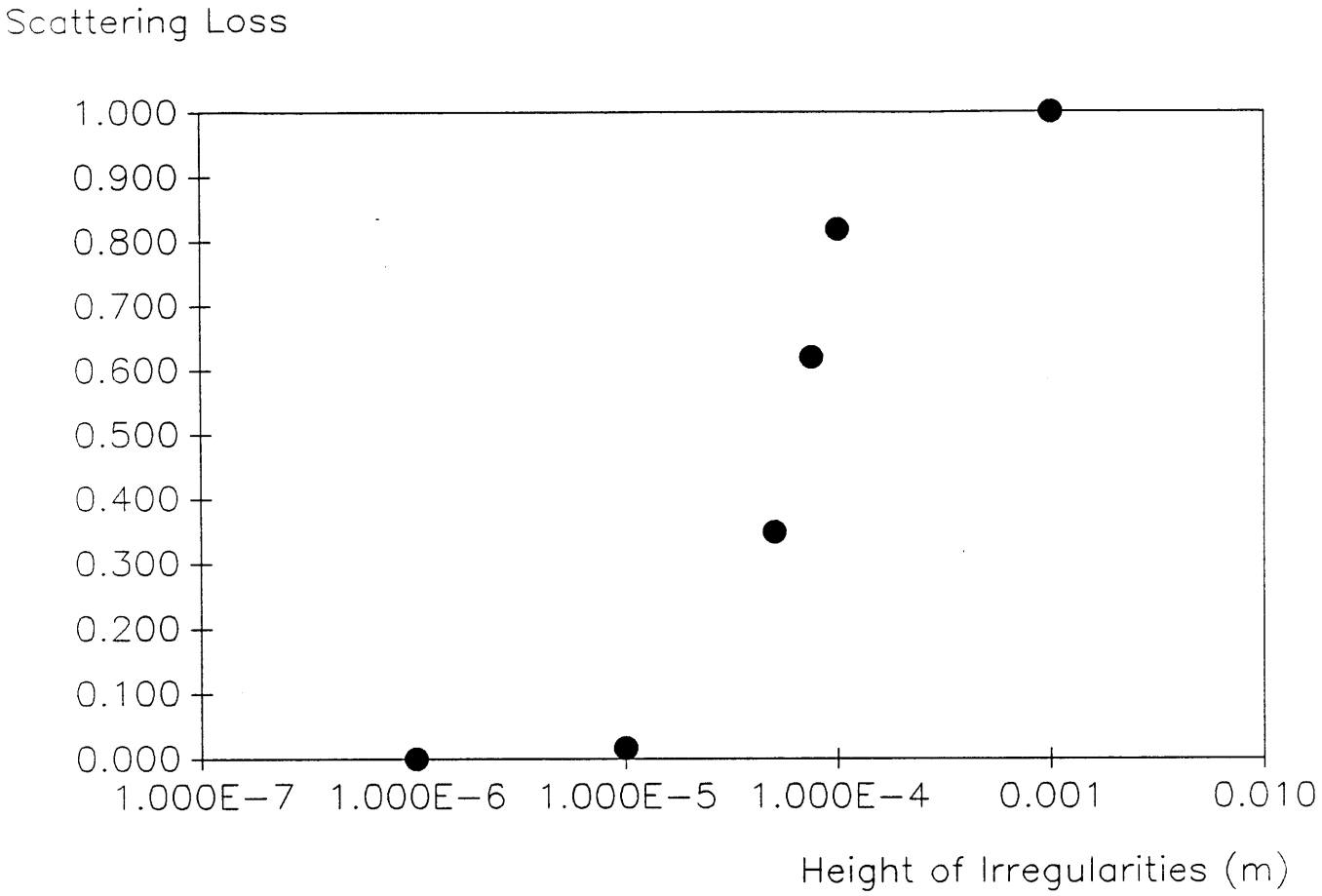

Figure III.A.3.1 Scattering loss vs. Height of surface irregularities

Assuming the correlation radius is 2 μ, the height of the surface irregularities is plotted against scattering loss. For a surface with irregularities of height less than 10 angstroms, it can be considered scattering loss free.

In Vinogradov's example, the incoming light beam is also 200 angstroms in wavelength. He rotated the light beam 90 degrees. His surface's microirregularities were 60 angstroms in height rms. He considered the surface to be smooth if the correlation radius ς is $\geq$ 1 μ, which agrees with our calculations. Figure III.A.3.2 plots the relationship between

irregularities' height and correlation radius.

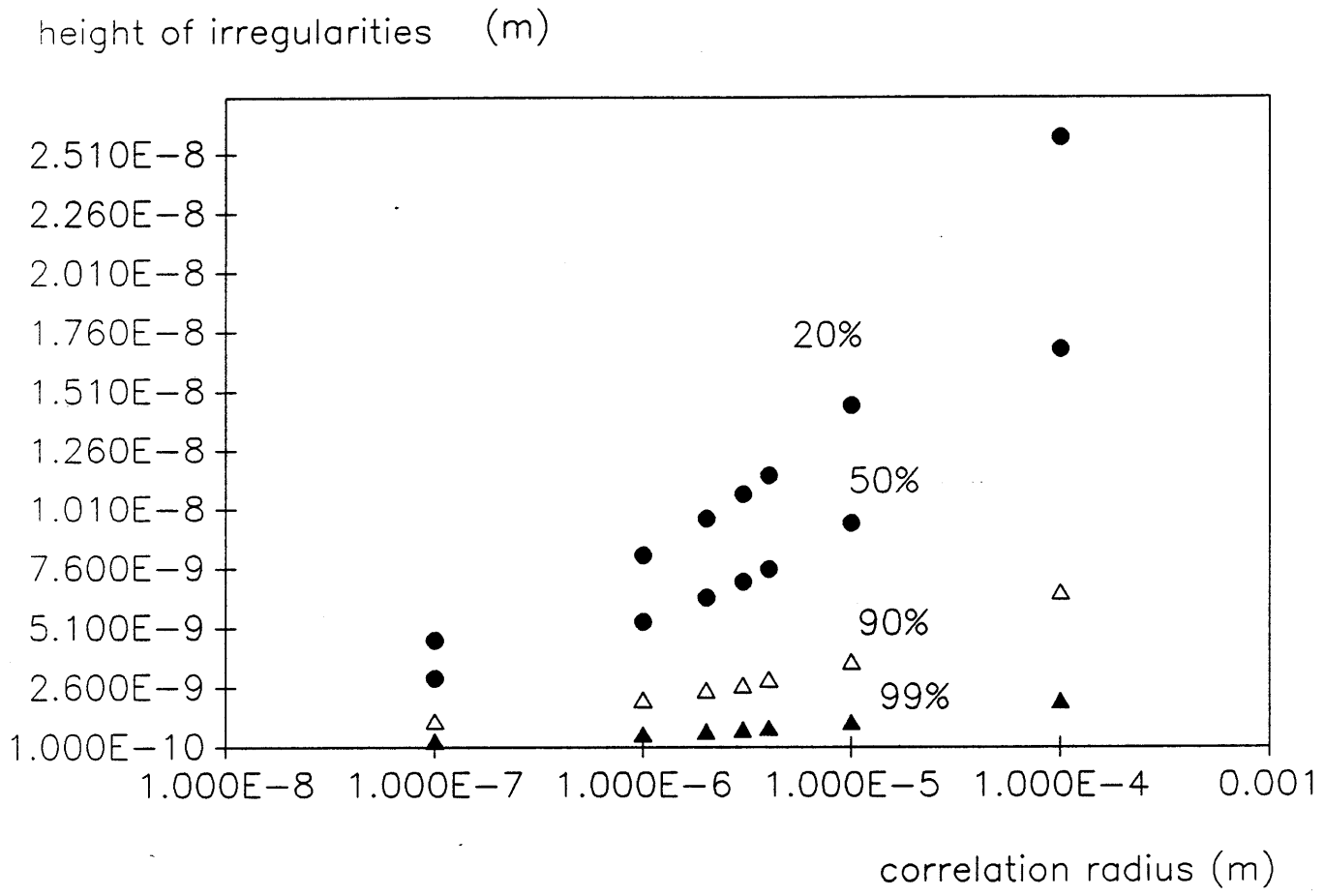

Figure III.A.3.2 Height vs. Correlation radius

The values of surface irregularities' height are plotted against their correlation radius for different (1 - scattering loss).

Practical issues that are involved in reducing microirregularities can discussed in Chapter 4. Obtaining smoothness on the order of hundreds of angstroms is easy. Obtaining smoothness of 10 angstroms require much more work and have only been carried out by very few industries.

III.A.4 Kramers-Kronig Analysis

The real part of the optical constant is related to the imaginary part of the optical constant by the Kramers-Kronig relation[1](50).

$$\kappa_r(\omega) - 1 = \frac{P}{\pi}\int_{-\infty}^{\infty} \frac{\kappa_i(\omega')}{\omega' - \omega} d\omega' \quad (III.A.4.1)$$

Therefore, if we know the real part of the optical constant, we also know the imaginary part and vice-versa. Kramers-Kronig have been used extensively to calculate the optical constants theoretically. It provides a good estimation for the energy range that we are interested in.

For energy above 100eV, the relationship for finding the optical constants become much simpler. The relationship is linear[2]. If we write the dielectric constant as a complex constant ϵ:

$$\epsilon = 1 - \delta - i\beta,$$

δ and β are related to the atomic scattering factor f_p,

$$\frac{\delta}{2} = \left(\frac{r_0}{2\pi}\right) \lambda^2 \phi \sum_p x_p f_{1p} \quad (III.A.4.2)$$

$$\frac{\beta}{2} = \left(\frac{r_0}{2\pi}\right) \lambda^2 \phi \sum_p x_p f_{2p} \quad (III.A.4.3)$$

where f_{1p} and f_{2p} designate the real part and imaginary part of the scattering factor, respectively and ϕ is the number of molecular groups per unit volume each with x_p atoms.

The experimental data for photoabsorption cross section for 100eV and above have been compiled by Henke, B.L. for all elements[2]. Therefore, the optical constants can be much more easily obtained for energy of that range.

III.A.4.1 Kramers-Kronig's relation

We have been setting up the program to use Kramers-Kronig to calculate the optical constants of all material at energy range below 100eV. We describe the Kramers-Kronig briefly below.

The analyticity of the optical constant, κ, in the upper half plane of ω allows the use of the Cauchy's theorem to relate the imaginary and real parts of κ as shown in Eq. (III.A.4.1). The real part of the optical constant is related to the total cross section σ_t

$$\kappa_r(\omega) - 1 = 2\frac{cN}{\pi} P \int_{-\infty}^{\infty} \frac{\sigma_t(\omega')}{\omega'^2 - \omega^2} d\omega' \quad (III.A.4.1.1)$$

where the total cross section is composed of both the absorption cross section, σ_a, and the scattering cross section, σ_s [3]

$$\sigma_t = \sigma_a + \sigma_s \quad (III.A.4.1.2)$$

The scattering cross section can be shown to be negligible compared to the absorption cross section. Consequently, we shall worry only about contribution due to only the the absorption cross section. We can rewrite Eq.(III.A.4.1.1)

$$\kappa_r(\omega) - 1 \approx 2\frac{cN}{\pi} P \int_{0}^{\infty} \frac{\sigma_a(\omega')}{\omega'^2 - \omega^2} d\omega' \quad (III.A.4.1.3)$$

The equation becomes singular at ω. We can resolve this singularity by subtracting the singular value from the integrand,

$$\int_0^\infty \frac{\sigma_a(\omega') - \sigma_a(\omega)}{\omega'^2 - \omega^2} d\omega' + \int_0^\infty \frac{\sigma_a(\omega')}{\omega'^2 - \omega^2} d\omega' \quad (III.A.4.1.4)$$

The first term can be calculated by numerical integration, and the second term can be evaluated analytically. In addition, we will truncate the integration interval for the first integrand at which the absorption cross section starts to decrease.

$$\int_{\omega_{max}}^\infty \frac{\sigma_a(\omega_{max})}{\omega'^2 - \omega^2} d\omega' \quad (III.A.4.1.6)$$

Most photoabsorption cross section may have steep slope. To approximate such high rate of change, the quadrature that we use will follows Simpson's $\frac{1}{3}$ rule.

III.A.4.2 Utilization of the Cooper Minimum

For a specific wavelength that we wish to design the mirror for, we want to use elements that has their Cooper Minimum at that or close to that specific wavelength. Basically, Cooper Minimum is the point at which the photoabsorption cross section of the element is at its Minimum. If the element absorbs less, it reflects more.

J. W. Cooper used a nonhydrogenic model with central field to describe the absorption-edge-like phenomenon in lower energy (between threshold and a few hundreds of eV)[4-7]. Cooper Minima is due to the zero of the photoionization matrix element. It is an interference effect.

For 200 angstroms, which correspond approximately to 64eV, both thorium and barium

displays a Cooper Minimum at that energy level. (See Figure III.A.4.1)

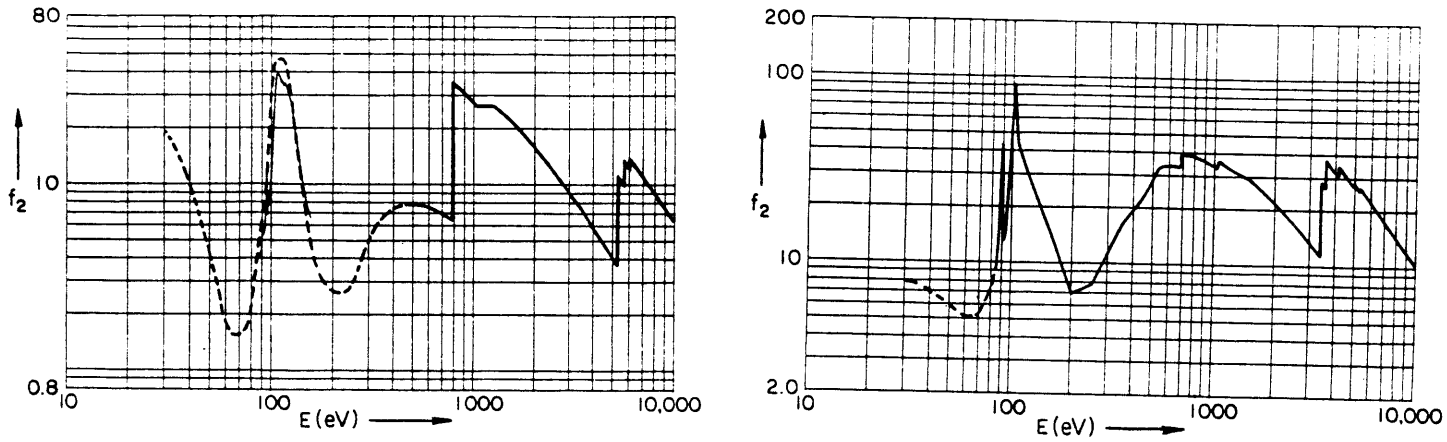

Figure III.A.4.1

The Cooper Minima, which occur at less than 100eV for both Ba, plot on the left, and Th, plot on the right has a much gentler slope than the absorption edges, which appear as sharp peaks at the higher energy levels.

III.A.4.3 Selection of material for our WGM mirror design

The wavelength for which we want to build a whispering gallery mirror for is approximately 195 angstroms.

The following criteria are used in narrowing down the elements.

1. It should not be radioactive

2. It should not oxidize easily (especially on the outer few angstroms, because the skin depth is on the order of angstroms)

3. It should serve as a good thin film coating (malleable; not brittle)

Besides the criteria cited above, the element should be within budgetary constraints. Of all the elements listed, none of them is beyond reach. Some elements are toxic. However,

since highly toxic elements, such as Ga and As, have been successfully handled in labs, toxicity does not serve as a major criteria.

The following survey shows the properties of the elements that has their Cooper Minimum in the soft x-rays.

The final three elements that we are considering are molybdenum, strontium, and zirconium.

\relax

Z	Element	toxic	oxidizes in air	radioactive	brittle	physical forms	λ_{rel}
36	Kr	no	N/A	no	N/A	gas	178Å
37	Rb	no	yes	yes	no		155Å
38	Sr	no	yes	no	no		153Å
39	Y	no	yes	no	no		104Å
40	Zr	no	no	no	no		113Å
41	Nb	no	yes	no	no		113Å
42	Mo	no	high temp	no	no		116Å
43	Tc	no	no	yes	N/A	liquid	146Å
44	Ru	no	high temp	no	no	ductile	116Å
45	Rh	no	no	no	no		116Å
46	Pd	no	no	no	no	ductile	88.8Å
47	Ag	no	air with ozone and sulfur		no	no	96Å
48	Cd	yes	no	no	no		83Å
49	In	low	yes	no	no	wets glass	73Å
50	Sn	no	low temp	no	no		78Å
51	Sb	yes	high temp	no	no		62Å
52	Te	yes	yes	yes	no		62Å
53	I	no	no	no	no	volatile	62Å
54	Xe	no	N/A	no	N/A	gas	249Å
55	Cs	no	yes	no	N/A	liquid	244Å
56	Ba	yes	yes	no	yes		191Å
57	La	low-med	yes	no	no		173Å
58	Ce	no	yes	no	no		155Å

59	Pr	no	yes	no	no		124Å
60	Nd	low-med	yes	no	no		105Å
61	Pm	no	no	yes	N/A	liquid	138Å
62	Sm	unknown	high temp	no	no		153Å
63	Eu	no	yes	no	no	costly	178Å
64	Gd	no	moist	no	no		88.8Å
65	Tb	unknown	no	no	no		85.7Å
66	Dy	no	no	no	no		88.8Å
67	Ho	low-med	moist	no	no		82.9Å
68	Er	no	no	no	no		113Å
69	Tm	no	moist	no	no		70.6Å
70	Yb	low-med	yes	no	no		248Å
71	Lu	low	no	yes	no	costly	137Å
72	Hf	yes	high temp	no	no		178Å
73	Ta	no	high temp	yes	no		155Å
74	W	no	yes	no	no		155Å
75	Re	unknown	no	no	no	ductile	124Å
76	Os	no	no	no	yes		138Å
77	Ir	no	no	no	yes		143Å
78	Pt	no	no	no	no		105Å
79	Au	no	no	no	no		95.6Å
80	Hg	yes	no	no	N/A	liquid	77.7Å
81	Tl	no	yes	no	no		77.7Å
82	Pb	yes	no	no	no		76.3Å
83	Bi	no	no	no	yes		67.2Å
84	Po	no	no	yes	no	volatile	62.2Å
85	At	no	no	yes	no		59.8Å
86	Rn	no	N/A	yes	N/A	gas	296Å
87	Fr	no	no	yes	N/A	liquid	303Å

88	Ra	no	no	yes	no		310Å
89	Ac	no	no	yes	no		248Å
90	Th	no	no	yes	no		204Å
91	Pa	yes	no	yes	no		141Å
92	U	no	no	yes	no		132Å
93	Np	no	no	yes	no	synth.	143Å
94	Pu	no	no	yes	no	synth.	138Å

III.B Theoretical Design of the Whispering Gallery Mirrors

III.B.1 Finite Element Analysis of 2D Helmholtz Equation for An Arbitrarily Shaped Surface

In our design, we want to solve the Green's function for an arbitrarily shaped surface. We will do so through a finite-element approach. We cut a surface into small pieces. On each piece, there is a field E_j associated with it. To visualize the E field more easily, we can define a new set of coordinate for each piece. $\hat{\xi}_1$ is parallel to the piece; $\hat{\xi}_2$ is normal

to the piece[1-3].

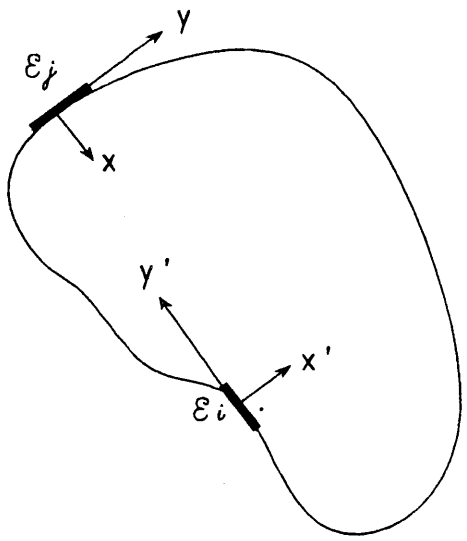

Figure III.B.1

An arbitrarily shaped surface can be described by finite elements. A new set of coordinates, one is normal to the finite element, and the other parallel, can be defined to describe each element

where they are transformed from the x and y axis in the following way:

$$\xi_1 = x\cos\psi + y\sin\psi$$

$$\xi_2 = -x\sin\psi + y\cos\psi$$

According to the Helmholtz's equation, the contribution of E_i to E_j is

$$E_i^{(j)}(\xi_1, \xi_2) = \int_{-\infty}^{\infty} dz \int_{-\delta}^{\delta} d\xi_2 E_j(\xi_1, \xi_2) \cdot \frac{\partial}{\partial \xi_1} \frac{e^{ik[(\xi_1-\xi_{1j})^2+(\xi_2-\xi_{2j})^2+z^2]^{\frac{1}{2}}}}{[(\xi_1-\xi_{1j})^2+(\xi_2-\xi_{2j})^2+z^2]^{\frac{1}{2}}}$$

$$-\frac{e^{ik[(\xi_1-\xi_{1j})^2+(\xi_2-\xi_{2j})^2+z^2]^{\frac{1}{2}}}}{[(\xi_1-\xi_{1j})^2+(\xi_2-\xi_{2j})^2+z^2]^{\frac{1}{2}}}\cdot\frac{dE_j(\xi_1,\xi_2)}{d\xi_1} \qquad (III.B.1.1)$$

where we have assumed that the field does not vary along the z-axis. As stated by the Huygen's principle (as mentioned in Appendix D), if we know how each piece is related to one another, we can solve for the E field on the boundary and within the surface by solving each of the piece self-consistently. At this point, we will concentrate on simplifying (III.B.1.1) rather than solving the matrix itself.

We can rearrange the terms in (III.B.1.1),

$$E_i^{(j)}(\xi_1,\xi_2)=\int_{-\delta}^{\delta}d\xi_2 E_j(\xi_1,\xi_2)\frac{\partial}{\partial\xi_1}\int_{-\infty}^{\infty}dz\frac{e^{ik[(\xi_1-\xi_{1j})^2+(\xi_2-\xi_{2j})^2+z^2]^{\frac{1}{2}}}}{[(\xi_1-\xi_{1j})^2+(\xi_2-\xi_{2j})^2+z^2]^{\frac{1}{2}}}$$
$$-\int_{-\delta}^{\delta}d\xi_2\frac{dE_j(\xi_1,\xi_2)}{d\xi_1}\int_{-\infty}^{\infty}dz\frac{e^{ik[(\xi_1-\xi_{1j})^2+(\xi_2-\xi_{2j})^2+z^2]^{\frac{1}{2}}}}{[(\xi_1-\xi_{1j})^2+(\xi_2-\xi_{2j})^2+z^2]^{\frac{1}{2}}} \qquad (III.B.1.2)$$

We can evaluate the expression along the z-axis. We are evaluating the expression,

$$\int_{-\infty}^{\infty}\frac{e^{ik[(\xi_1-\xi_{1j})^2+(\xi_2-\xi_{2j})^2+z^2]^{\frac{1}{2}}}}{[(\xi_1-\xi_{1j})^2+(\xi_2-\xi_{2j})^2+z^2]^{\frac{1}{2}}}dz \qquad (III.B.1.3)$$

Since variables ξ_1 and ξ_2 act as constants in this expression, we can make the folowing substitution,

$$a^2=(\xi_1-\xi_{1j})^2+(\xi_2-\xi_{2j})^2$$

Equation (II.3) becomes,

$$\int_{-\infty}^{\infty}dz\frac{e^{ik[a^2+z^2]^{\frac{1}{2}}}}{(a^2+z^2)^{\frac{1}{2}}} \qquad (III.B.1.4)$$

We can expand the exponential into cos's and sin's,

$$\int_{-\infty}^{\infty}dz\frac{e^{ik[a^2+z^2]^{\frac{1}{2}}}}{(a^2+z^2)^{\frac{1}{2}}}$$

$$= \int_{-\infty}^{\infty} dz \frac{cosk(a^2+z^2)^{1/2}}{(a^2+z^2)^{1/2}} + i\int_{-\infty}^{\infty} dz \frac{sink(a^2+z^2)^{1/2}}{(a^2+z^2)^{1/2}}$$

$$= 2\int_{0}^{\infty} dz \frac{cosk(a^2+z^2)^{1/2}}{(a^2+z^2)^{1/2}} + 2i\int_{0}^{\infty} dz \frac{sink(a^2+z^2)^{1/2}}{(a^2+z^2)^{1/2}} \qquad (III.B.1.5)$$

due to the integrands' evenness.

We can make another substitution to simplify the integral. Let

$$u^2 = a^2 + z^2$$

(II.5) becomes,

$$2\int_{a}^{\infty} du \frac{cosku}{(u^2-a^2)^{\frac{1}{2}}} + 2i\int_{a}^{\infty} du \frac{sinku}{(u^2-a^2)^{\frac{1}{2}}} \qquad (III.B.1.6)$$

Equation (II.6) is evaluated to be

$$-\sqrt{\pi}\Gamma\left(\frac{1}{2}\right) N_0(ka) + i\sqrt{\pi}\Gamma\left(\frac{1}{2}\right) J_0(ka)$$

an expression that can be simplified to the Hankel's function expression. (II.3) is equivalent to

$$i\pi H_0^{(1)}(ka) \qquad (III.B.1.7)$$

We can substitute (II.7) back into our original equation, we arrive at

$$E_i^{(j)}(\xi_1,\xi_2) = \int_{-\delta}^{\delta} d\xi_2 E_j(\xi_1,\xi_2) \cdot \frac{\partial}{\partial \xi_1} i\pi H_0^{(1)}(k[(\xi_1-\xi_{1j})^2 + (\xi_2-\xi_{2j})^2])$$

$$-\int_{-\delta}^{\delta} d\xi_2 \frac{dE_j(\xi_1,\xi_2)}{d\xi_1} \cdot i\pi H_0^{(1)}(k[(\xi_1-\xi_{1j})^2 + (\xi_2-\xi_{2j})^2]) \qquad (III.B.1.8)$$

Most of the time we are interested in how many wavelengths do each piece contain, that is, we are interested in ka and not a itself. We can substitute the following expressions,

$$\sigma_1^2 = k^2(\xi_1-\xi_{1j})^2 \qquad (III.B.1.9.1)$$

$$\sigma_2^2 = k^2(\xi_2 - \xi_{2j})^2 \qquad (III.B.1.9.2)$$

$$\xi_1 = \left(\frac{\sigma_1^2}{k^2}\right)^{\frac{1}{2}} + \xi_{1j} \qquad (III.B.1.9.3)$$

$$\xi_2 = \left(\frac{\sigma_2^2}{k^2}\right)^{\frac{1}{2}} + \xi_{2j} \qquad (III.B.1.9.4)$$

$$2\sigma_1 d\sigma_1 = 2(\xi_1 - \xi_{1j})d\xi_1 \qquad (III.B.1.9.5)$$

$$2\sigma_2 d\sigma_2 = 2(\xi_2 - \xi_{2j})d\xi_2 \qquad (III.B.1.9.6)$$

so that,

$$d\xi_1 = \frac{\sigma_1}{\left(\frac{\sigma_1}{k}\right)} d\sigma_1 \qquad (III.B.1.9.7)$$

$$d\xi_2 = \frac{\sigma_2}{\left(\frac{\sigma_2}{k}\right)} d\sigma_2 \qquad (III.B.1.9.8)$$

we can rewrite (II.8) in the following manner:

$$\int_{k(-\delta-\xi_{1j})}^{k(\delta-\xi_{1j})} k d\sigma_2 E_j(\sigma_1,\sigma_2)\left(k \cdot i\pi \frac{\partial}{\partial\sigma_1} H_0^{(1)}([\sigma_1^2+\sigma_2^2]^{\frac{1}{2}})\right)$$
$$-\int_{k(-\delta-\xi_{1j})}^{k(\delta-\xi_{1j})} k d\sigma_2 \left(\frac{dE_j(\sigma_1,\sigma_2)}{d\sigma_1}\cdot k\right) i\pi \frac{\partial}{\partial\sigma_1} H_0^{(1)}([\sigma_1^2+\sigma_2^2]^{\frac{1}{2}}) \qquad (III.B.1.10)$$

III.B.2 Analysis of 2D Helmholtz for High Frequency Approximations

Essentially, we wish to solve the result we obtained in Section III.B.1 for all frequencies. We want to simplify Eq. (III.B.10). We can take two different approximations: the high frequency approximation and the low frequency approximation. Physically the high frequency approximation correspond to solution for uv or x-rays. On the other hand, the low frequency approximation correspond to infrared light beams.

In this section, let us examine the integral using asymptotic high frequency approximation, we get

$$\int_{-\delta}^{\delta} H_0\left(k(x-x')\right) e^{i\eta x'} dx' = \frac{1}{\pi}\int_C dz \int_{-\delta}^{\delta} dx' e^{i\eta x} e^{ik(x-x')cosz}$$

$$= \frac{1}{\pi}\int_C dz e^{ikxcosz} \int_{-\delta}^{\delta} dx' e^{ikx'cosz + i\eta x'}$$

$$= \frac{1}{\pi}\int_C dz e^{ikxcosz}\left[\frac{1}{\eta - kcosz}\right]\left[\frac{e^{i(\eta-kcosz)\delta} - e^{-i(\eta-kcosz)\delta}}{i}\right]$$

$$= \frac{1}{i\pi}\int_C dz \frac{e^{i(kxcosz - k\delta cosz + \eta\delta)} - e^{-i(kxcosz - k\delta cosz + \eta\delta)}}{\eta - kcosz} \qquad (III.B.2.1)$$

If we evaluate the first term of the integral in (III.B.2.1), we arrive at

$$\frac{1}{i\pi} e^{i\eta\delta} \int_C \frac{e^{i(kxcosz - k\delta cosz)}}{\eta - kcosz} dz \qquad (III.B.2.2)$$

z is a complex number, i.e.,

$$z = u + iv \qquad (III.B.2.3)$$

Moreover, we have satisfy the condition that it is constant phase; consequently,

$$i\left(kxcosz - k\delta cosz\right)$$

is real.

$$cos\,(u+iv) = cosucoshv + isinusinhv \qquad (III.B.2.4)$$

and that

$$cosucoshv = 1$$

Therefore, we arrive at the result,

$$\frac{1}{i\pi} e^{i\eta\delta} e^{ik(x-\delta)} \int_{C'} \frac{e^{-k\delta sinusinhv}}{\eta - k - isinusinhv} dz (III.B.2.5)$$

If we substitute ξ for $sinusinhv$, we obtain,

$$\frac{1}{i\pi} e^{i\eta\delta} e^{ik(x-\delta)} \int_{-\infty}^{\infty} \frac{e^{-k\delta(x-\delta)\xi}}{\eta - k - i\xi} \frac{d\xi}{O(\xi)} \qquad (III.B.2.6)$$

$$dz = \frac{1 + i\left(\frac{1}{cosx}\right)^2 sinx}{sinh\left(cosh^{-1}\left(\frac{1}{cosx}\right)\right)} dx \qquad (III.B.2.7)$$

$$d\xi = cosxsinhy + sinxcoshy \frac{dy}{dx} dx \qquad (III.B.2.8)$$

$$d\xi = \left[cosxsinh\left(cosh^{-1}\left(\frac{1}{cosx}\right)\right) + sinx\left(\frac{1}{cosx}\right) \frac{\left(\frac{1}{cosx}\right)^2 sinx}{sinh\left(cosh^{-1}\left(\frac{1}{cosx}\right)\right)} \right] dx \qquad (III.B.2.9)$$

Therefore,

$$d\xi = dz \left[\frac{cosxsinh\left(cosh^{-1}\left(\frac{1}{cosx}\right)\right) + \frac{tan^2 x}{cosx \frac{1}{sinh\left(cosh^{-1}\left(\frac{1}{cosx}\right)\right)}}}{\frac{1+\left(\frac{1}{cosx}\right)^2 sinx}{sinh\left(cosh^{-1}\left(\frac{1}{cosx}\right)\right)}} \right] \qquad (III.B.2.10)$$

$$O(\xi) = \frac{d\xi}{dz} \qquad (III.B.2.11)$$

We can try to simplify the expression $sinh\left(cosh^{-1}\left(\frac{1}{cosx}\right)\right)$.

Let

$$a = \frac{1}{cosx + \left(\frac{1}{cos^2x+1}\right)^{\frac{1}{2}}} \qquad (III.B.2.12)$$

and let

$$a = g + \sqrt{g^2+1} \qquad (III.B.2.13)$$

, we get

$$f + \sqrt{f^2+1} = g + \sqrt{g^2+1} \qquad (III.B.2.14)$$

$$\left(f + \sqrt{f^2+1}\right)\left(f - \sqrt{f^2+1}\right) = a\left(f - \sqrt{f^2+1}\right) \qquad (III.B.2.15)$$

$$f + \sqrt{f^2+1} = a \qquad (III.B.2.16.1)$$

$$f - \sqrt{f^2+1} = -\frac{1}{a} \qquad (III.B.2.16.2)$$

$$f = \frac{1}{2}\left(a - \frac{1}{a}\right) \qquad (III.B.2.16.3)$$

or that,

$$f = \frac{1}{2}\,\frac{1}{cosx} + \sqrt{\frac{1}{cos^2x+1}} - \frac{1}{\frac{1}{cosx} + \sqrt{\frac{1}{cos^2x+1}}} \qquad (III.B.2.16.4)$$

$d\xi$ becomes

$$d\xi = dz \frac{\frac{\frac{1}{2}\left[\frac{1+\sqrt{1+cos^2x-cos^2x}}{1+\sqrt{cos^2x}}\right]+2tan^2x}{cosx\frac{1}{\frac{1}{2}\,cosx}}}{\frac{1+2\left(\frac{1}{cosx}\right)^2 sinx}{\frac{2}{cosx}}}$$

$$= dz\frac{1+tan^2x}{1+tanx}$$

$$= dz\frac{1}{cosx\,(sinx+cosx)} \qquad (III.B.2.17)$$

$$\xi = sinx \cdot \frac{1}{2} \cdot \left[\frac{\frac{1}{cosx} + \frac{1}{cosx}\sqrt{1+cos^2x} - cosx}{\frac{1}{\sqrt{cos^2x+1}}}\right] \qquad (III.B.2.18)$$

III.B.3 Analysis of the 2D Helmholtz Equation Using Steepest Descent Approximation

Another approach to evaluate the Helmholtz's equation for high frequency fields is to take its steepest descent approximation. We start with the equation:

$$\frac{1}{i\pi}\frac{e^{i\eta\delta}}{\eta - kcosz}\int_C e^{ik(x-\delta)cosz}dz \qquad (III.B.3.1)$$

For large z we can expand $cosz$ into its Taylor's series expansion in the exponential in the numerator, while ignoring and making it unity in the denominator:

$$\frac{1}{i\pi}\frac{e^{i\eta\delta}e^{ik(x-\delta)}}{\eta - k}\int_C cosk\,(x-\delta)\,\frac{z^2}{2} - isink\,(x-\delta)\,\frac{z^2}{2}dz \qquad (III.B.3.2)$$

We can expand the exponential term into sin and cos terms, so that Eq(III.B.3.2) becomes:

$$\frac{1}{i\pi}\frac{e^{i\eta\delta}e^{ik(x-\delta)}}{\eta - k}\int_C \frac{1}{\sqrt{k\,(x-\delta)\,\left(\frac{1}{2}\right)}}\left(cosu^2 - isinu^2\right)du \qquad (III.B.3.3)$$

To evaluate the integral expressions, we can make a substitution such that :

$$u^2 = k(x-\delta)\frac{z^2}{2} \qquad (III.B.3.4)$$

With this replacement of variable, Eq (III.B.3.3) becomes:

$$\frac{1}{\pi}\frac{e^{i\eta\delta}e^{ik(x-\delta)}}{\eta-k}\frac{1}{\sqrt{k\left(x-\delta\right)\left(\frac{1}{2}\right)}}\sqrt{\frac{\pi}{2}}\left[S\left(u^2\right)-iC\left(u^2\right)\right]|_C (III.B.3.5)$$

We evaluate the integral between

$$-\frac{\pi}{2}\cdot\frac{k\left(x-\delta\right)}{2} and -\frac{\pi}{2}\cdot\frac{k\left(x-\delta\right)}{2}$$

. We can, expand the expression to

$$=\frac{1}{\pi}\frac{e^{i\eta\delta}e^{ik(x-\delta)}}{\eta-k}\frac{1}{\sqrt{k\left(x-\delta\right)\left(\frac{1}{2}\right)}}\sqrt{\frac{\pi}{2}}\left[S\left(u^2\right)-iC\left(u^2\right)\right]\Big|_{-\frac{\pi}{2}\cdot\frac{k(x-\delta)}{2}}^{\frac{\pi}{2}\cdot\frac{k(x-\delta)}{2}}$$

$$=\frac{1}{\pi}\frac{e^{i\eta\delta}e^{ik(x-\delta)}}{\eta-k}\frac{1}{\sqrt{k\left(x-\delta\right)\left(\frac{1}{2}\right)}}\sqrt{\frac{\pi}{2}}\times$$

$$\cdot\frac{1}{\sqrt{2\pi}}\left[\int_0^{\frac{\pi}{2}\cdot\frac{k(x-\delta)}{2}}\frac{sinu^2}{u}du+\int_{\frac{-\pi}{2}\cdot\frac{k(x-\delta)}{2}}^0\frac{sinu^2}{u}du\right.$$

$$\left.+i\int_0^{\frac{\pi}{2}\cdot\frac{k(x-\delta)}{2}}\frac{sinu^2}{u}du-i\int_{\frac{-\pi}{2}\cdot\frac{k(x-\delta)}{2}}^0\frac{cosu^2}{u}du\right] (III.B.3.6)$$

Due to the evenness of the integral expressions in (II.8), we obtain,

$$\frac{1}{\pi}\frac{e^{i\eta\delta}e^{ik(x-\delta)}}{\eta-k}\frac{1}{\sqrt{k\left(x-\delta\right)\left(\frac{1}{2}\right)}}\sqrt{\frac{\pi}{2}}x$$

$$\cdot\left[\int_0^{\frac{\pi}{2}\cdot\frac{k(x-\delta)}{2}\frac{1}{\sqrt{\frac{\pi}{2}}}}cos\left(\frac{\pi}{2}t^2\right)dt-i\int_0^{\frac{\pi}{2}\cdot\frac{k(x-\delta)}{2}\frac{1}{\sqrt{\frac{\pi}{2}}}}sin\left(\frac{\pi}{2}t^2\right)\right]dt (III.B.3.7)$$

We can expand the expression into *sin* and *cos* terms,

$$\frac{-i}{\pi}\frac{1}{\eta-k}\left(cos\eta\delta+isin\eta\delta\right)\left(cosk\left(x-\delta\right)+isink\left(x-\delta\right)\right)\cdot\frac{1}{\sqrt{k\left(x-\delta\right)\left(\frac{1}{2}\right)}}\times$$

$$2\sqrt{\frac{\pi}{2}}\int_0^{\frac{\pi}{2}\cdot\frac{k(x-\delta)}{2}\frac{1}{\sqrt{\frac{\pi}{2}}}}cos\left(\frac{\pi}{2}t^2\right)dt-i\int_0^{\frac{\pi}{2}\cdot\frac{k(x-\delta)}{2}\frac{1}{\sqrt{\frac{\pi}{2}}}}sin\left(\frac{\pi}{2}t^2\right)dt (III.B.3.8)$$

which is expanded to,

$$\frac{-i}{\pi}\frac{1}{\eta-k}\left[i\left(cos\eta\delta cosk\left(x-\delta\right)-\left(sin\eta\delta sink\left(x-\delta\right)\right)-\left(cos\eta\delta sink\left(x-\delta\right)+cosk\left(x-\delta\right)sin\eta\delta\right)\right]\times$$

$$2\sqrt{\frac{\pi}{2}}\int_0^{\frac{\pi}{2}\cdot\frac{k(x-\delta)}{2}}\frac{1}{\sqrt{\frac{\pi}{2}}}cos\left(\frac{\pi}{2}t^2\right)dt-i\int_0^{\frac{\pi}{2}\cdot\frac{k(x-\delta)}{2}}\frac{1}{\sqrt{\frac{\pi}{2}}}sin\left(\frac{\pi}{2}t^2\right)dt(III.B.2.9)$$

To evaluate (IIII.B.2.9), we need to break the expressions to real and imaginary parts.

$$\frac{-i}{\pi}\frac{1}{\eta-k}\cdot 2\sqrt{\frac{\pi}{2}}\left[-\left[cos\eta\delta sink(x-\delta)+cosk(x-\delta)sin\eta\delta\right]\int_0^{\frac{\pi}{2}\cdot\frac{k(x-\delta)}{2}}\frac{1}{\sqrt{\frac{\pi}{2}}}cos\left(\frac{\pi}{2}t^2\right)dt\right.$$

$$+\left[cos\eta\delta cosk(x-\delta)-sink(x-\delta)sin\eta\delta\right]\int_0^{\frac{\pi}{2}\cdot\frac{k(x-\delta)}{2}}\frac{1}{\sqrt{\frac{\pi}{2}}}sin\left(\frac{\pi}{2}t^2\right)dt$$

$$+i\left[cos\eta\delta sink(x-\delta)+cosk(x-\delta)sin\eta\delta\right]\int_0^{\frac{\pi}{2}\cdot\frac{k(x-\delta)}{2}}\frac{1}{\sqrt{\frac{\pi}{2}}}sin\left(\frac{\pi}{2}t^2\right)dt$$

$$\left.+i\left[cos\eta\delta cosk(x-\delta)-sink(x-\delta)sin\eta\delta\right]\int_0^{\frac{\pi}{2}\cdot\frac{k(x-\delta)}{2}}\frac{1}{\sqrt{\frac{\pi}{2}}}cos\left(\frac{\pi}{2}t^2\right)dt\right.\qquad(III.B.3.10)$$

IV. Implementation Issues

The following issues are involved in the construction of a whispering gallery mirror.

A. Cutting the surface

Making a spherical surface has become a standard task in machine shops and metal shops[1](55). In machine shops, the surface can be created within 2/1000 of an inch precision. The task itself can be done in a few hours. Many "higher-tech" machinery shops have diamond-turning, diamond-grinding machines. Those machines achieve approximately the same precision as that of the machines in machine shops operated by a skilled machinist. Therefore, the initial cutting of a spherical surface need not be accomplished by an expensive tool such as the diamond-grind machine, even though on the first thought it may be a more appealing machine to use to achieve higher precision.

To build other designs of the whispering gallery mirrors, the inner surface of the mirror has to have an aspheric curvature. To cut an aspheric surface, it is almost impossible to

cut it on the usual machineries found in machine shops. One of the following methods can be applied:

1. bend a surface (apply pressure)

2. diamond-grind it using a 2-axis machine (e.g. CNC 2-axis)[1]

B. Substrate Material Selection

In selecting the substrate material, the following criteria are being used:

1. Sturdiness

The material will not be easily squashed and bent, so that it will not break to pieces when it falls off of an optical bench.

2. Easy to be cut

The material would not splinter or leave off holes when cut by machinery[1]. The cut surface should be closed to an excellent polished surface quality.

3. Thermal tolerance

The material should moderate tolerance for heat. However, the incoming light does not carry too much energy. Therefore, the material need not to be high quality heat resistant.

C. Polishing the surface

There are two ways to polish the surface.

1. Use chemical compounds

For each material, a specific compound or a family of compounds can be used to polish the material[2](56). For aluminum, aluminum oxide is used to polish the surface. Aluminum oxide can also be used to polish many other metals: brass, hard chromium, copper, nickel and its alloys, steel and stainless steel, and zinc. The compound(s) cannot guarantee that the material can be polished to a smoothness on the order of tens of angstroms. Certain experimenters (such as) have developed specific compounds that can accomplish much

greater smoothness than the compounds mentioned above. However, they do not usually share the information. Moreover, these "in-house" compounds do not necessarily satisfy our stringent requirement.

2. Apply a nickel surface

In practice, nickel can be polished easily to a smoothness on the order of tens of angstroms[3](57). Therefore, we can apply such a nickel surface and polish this surface to our specification.

D. Distortion due to stress

The metal is subject to mechanical stress. However, the amount of distortion caused by the mechanical stress is not negligible.[1] Machinists have to wait enough time after the mechanical work in done on the piece for the stress to be relieved from the substrate. Only until then can the machinists detect the amount of distortion and make the corresponding corrections.

IV.A Construction of the Whisper Gallery Mirrors Locally

IV.A.I Constructing Mirrors of Smoothness on the Order of Angstroms

The experts for making mirrors that will be smooth on the order of tens of angstroms are the x-ray mirror groups in Perkin-Elmers and in Zeiss.[1,2] The HEAO-2 group in Perkin-Elmers is known for sending the first x-ray telescope to space. (the size of the mirror) Scientists at HEAO-2 have been able to achieve smoothness on the order of angstroms. The group at Zeiss have been able to achieve similar precisions on a Wolter-I type mirror. Producing a mirror of smoothness of that order is painstaking.

The substrates used by HEAO-2 are fused quartz[1]. They were manufactured by *Hereaus Quartzschmelze* in West Germany. Preparation of these substrates require a 20 major steps which take ten months to complete. These steps ensure an absolute minimum of bubbles and imperfections in the substrate to minimize scatter. The residual bubbles, if they do occur, are made to occur at discrete intervals. The bubbles eventually become negligible when they are hidden behind the support structures.

The height of the surface roughness for the HEAO-2 X-Ray Telescope is specified to be less than 30 angstroms rms. The group has achieved a surface roughness of less than

21 angstroms on the average, with 14 angstroms minimum, and 25 angstroms maximum.

Scientists at Perkin-Elmers pointed out that it is easier to produce smaller mirrors than large ones due to their stiffness. (describe the process done at Perkin-Elmers).

Group at Zeiss also manufactured a similar x-ray optical device for the West German X-Ray satellite ROSAT[2]. As verified by x-ray scatter measurements performed in the 130 m long x-ray test facility PANTER at the Max-Planck-Institut fur Extraterrestrische Physik in Garching, the group has achieved surface roughness of less than 2.8 angstroms on the average, with 1.8 angstroms minimum and 3.7 angstroms maximum, with high reproducibility.

IV.A.2 Constructing Whisper Gallery Mirrors

The production of a mirror of smoothness on the order of tens of angstroms does not require the high-precision instrumentations comparable to that accomplished in Perkin-Elmers. Brookhaven National Laboratory (Takacs) have accomplished in-house production of mirrors of this smoothness[3]. Oak Ridge National Laboratory has produced mirror on the smoothness of 100 angstroms. A few industries can accomplish the task. At first conjecture, jewelry shops and metal shops should have the capacity to accomplish this project. However, they claim not being able to do so. A few places within the United States can accomplish the smoothness criteria for glass. General Optics, for one, can polish glass surface to roughness of less than 5 angstroms rms[4]. The scattering factor is less than 50 ppm. For metal smoothness, after a few months of scouting, the author is only able to find one such company. Diamond Electrooptics claim to be able to accomplish smoothness of 15 angstroms[3].

IV.B Surface quality

IV.B.I Experiments to test surface quality in Perkin-Elmers

Perkin-Elmers adopted the following strategy when they were manufacturing the HEAO-2 X-Ray Telescope[1]. First, they tried to achieve the surface quality needed on smaller mirrors. Once they did achieve the quality, they examine whether the same instrumentation and testing techniques can be used to produce larger mirrors. From hindsight, they discovered that the small mirrors do not have the problem of locked-in strain due to stiffening tooling and the poor repeatability on the air-bearing measuring station. Those are the two essential problems that the group faced when they tried to manufacture the large mirror. The locked-in strain was discovered later and removed. The mercury flotation test was adopted to replace the air-bearing measuring station.

The HEAO-2 group automated their fringe scanning and manual data reduction process to speed up the surface quality tests. They used FECO interferometry test and scanners to examine the surface quality. They used the following schedule to examine their surface quality[1] :

1. Scan X-ray mirror and fringe scanner toroidal test plate.
2. Reduce paper tape data with computer.
3. Check computer output to ensure input entered and read correctly.

4. Review sagittal and slope error outputs and prepare figuring and smoothing schedules.

5. Figure mirror with designated polishing laps in accordance with schedule.

6. Install annular end caps and submerge-polish (smooth surface) in accordance with schedule.

7. Clean X-ray mirror and replicate mirror and calibration flat.

8. Measure inside diameter 1.500 inches from each end.

9. Measure inside roundness 1.5 inches from each end.

10. Coat replicas with silver, test with FECO interferometer, and analyze data.

11. Compute δR and $\delta(\delta R)$ and determine clear aperture location.

12. Return to Step 1.

The FECO (Fringes of Equal Chromatic Order) interferometry test in Perkin-Elmers is modified to test aspheric surfaces. The scanners are limited by the size of the stylus. Usually the scanners can measure height greater than 25 angstroms[2]. FECO examines the multiple-beam fringe of equal chromatic order created by two partially silvered surfaces, one of which is the test surface and the other supersmooth reference surface ($\approx$ 8 angstroms). FECO interferometry can determine surface microirregularities as small as 8 angstroms[2]. Readers who are interested in the detailed setup can read Jean M. Bennett's paper on FECO interferometry.

IV.B.II Experiments to test surface quality in Whispering Gallery Mirrors

Diamond Electrooptics tests the surface of the mirror by Computer-Generated Holography (CGH)[3]. This technique have been studied by Lee, and Lohmann and Paris independently[4,5].

The instrument has been developed by Honeywell, Tropel and the University of Arizona.

IV.B.II.1 Description of CGH

The instrument generates a reference wavefront and matches the wavefront reflected by the aspheric test surface. There are five "arms" in the instrument : the source arm, the test arm, the relay arm, the reference arm, and the viewing arm[6,7,8].

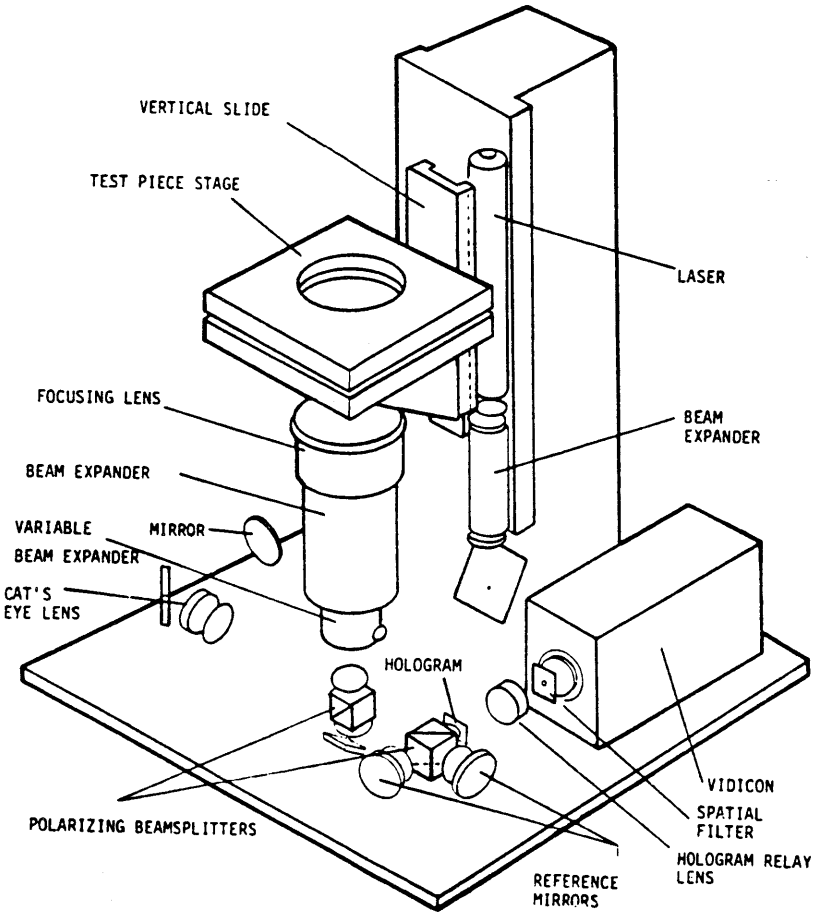

Figure IV.B.II.1 CGH Interferometer

The source arm controls the direction of the source beam by adjusting the half-wave plate. The polarized source beam is expanded and collimated. The beam encounters the first beamsplitter (BS-1). BS-1 reflects the S-polarized component, which serves as the reference beam. The transmitted P-polarized componenet thus serves as the test beam. A quarter-wave plate (QW), adjusts the polarization of the test beam and controls the test beam's transmittance.

The test surface reflects the test beam back to the vertical test arm, which is consisted of a series of interchangeable beam expanding and focusing lenses. The size of the beam can be adjusted by the variable beam expander.

The test beam is sent to the relay arm by the BS-1. It projects a real image of the test surface back through the beamsplitter toward the reference beam in the viewing arm.

The test beam and the reference beam are combined in the space between the two beamsplitters. However, they are still orthogonally oriented to each other. A second beamsplitter (BS-2) separates the two beams, reflecting the test beam along the axis of the viewing arm and transmits the reference beam.

The holographic image is contained in the viewing arm. The hologram is plotted by a

computer.

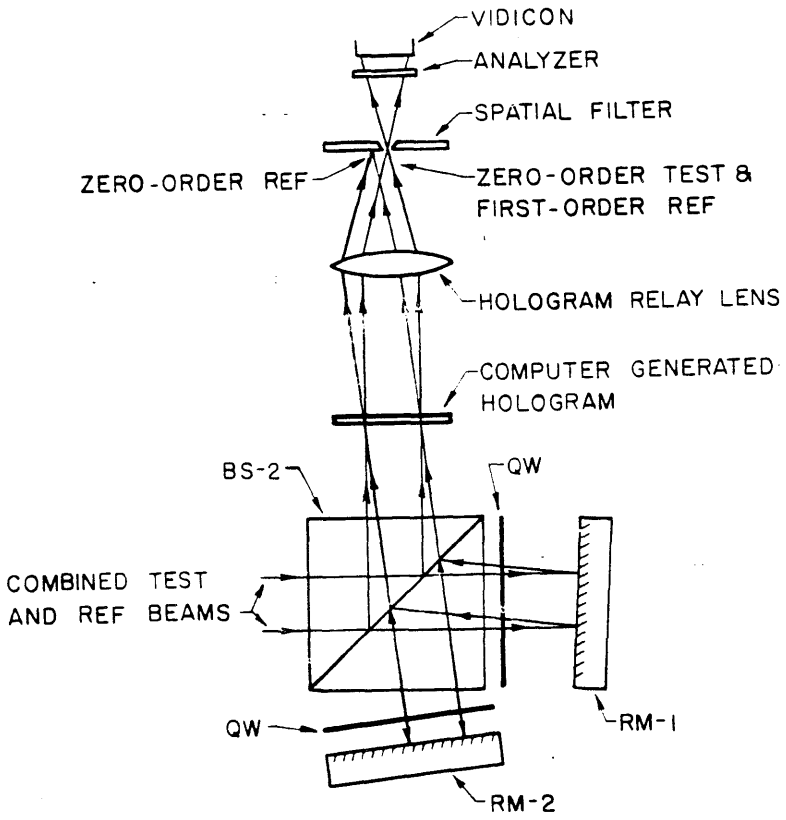

Figure IV.B.II.2 Viewing arm of CGH interferometer

It is a fringe pattern. Some of the test beam and the reference beam is diffracted by this hologram into plus and minus first-order beam. They are brought to focus on a white pinhole. The first-order reference beam and the zero-order test beam are superimposed if the reference beam if properly adjusted. The TV camera is behind the pinhole and records this superimposed image. The accuracy of this testing technique is limited by the

geometric accuracy of the hologram.

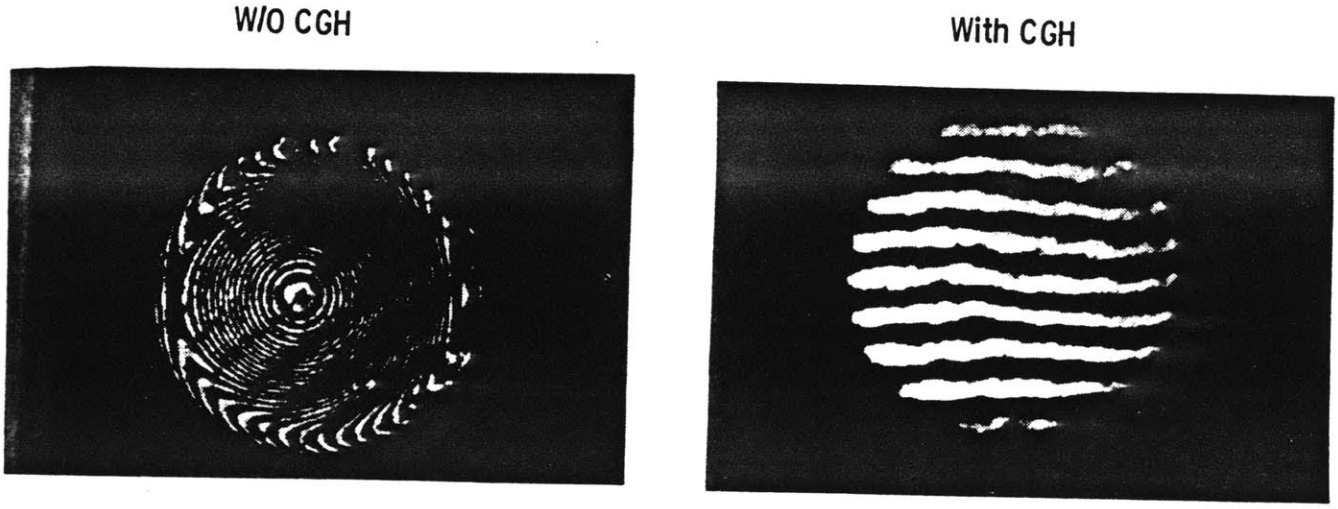

Figure IV.B.II.3 The left picture shows the fringe pattern without using CGH. The right picture shows the fring pattern with CGH

IV.B.II.1 Capabilities of CGH

CGH has overcome the limitation of the commercial optical recording devices by using direct e-beam writing on an electron-resist[8]. By using e-beam lithography, the number of pixels that can be used to write the holographic image can exceed 10^{10} due to the

submicron image resolution achievable.

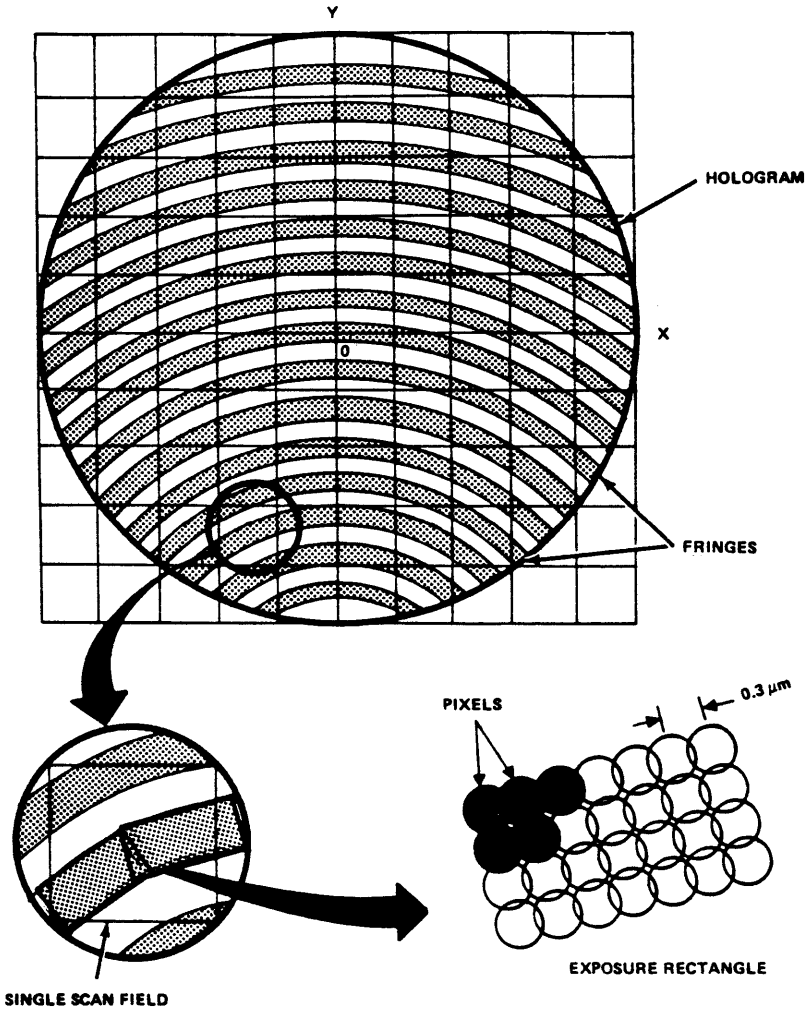

Figure IV.B.II.4

Holographic images are concatenation of little patches, shown in the inset. The accuracy of CGH depends on how small those patches can be and on how accurate those patches can be put together The sources of errors in e-beam direct writings are the followings: drift of the electron

optical axis due to contamination charging and stray fields; aberrations in electron optics; deviations from flatness and orthogonally of the mirrors on the workpiece stage. Honeywell

has achieved patterns with stitching errors of $\pm .15\mu$ in the x direction and $\pm .30\mu$ in the y direction. In storing the wave, it is only necessarily to store the phase information of the wave in this technique. For a typical hologram of 10 mm diameter, the image can be drawn in about 90 minutes.

V. Summary and Conclusions

This thesis surveys the both theoretical and experimental issues in building a whispering gallery mirror. It gives calculations and estimates for all issues in the design and implementation of the whispering gallery mirrors. Scattering losses, size of the incident angle, and skin depths were calculated to estimate the requirements to build a whispering gallery mirror for light source with a wavelength of 200 angstroms. The major issues in building a whispering gallery mirror were examined in detail. Schemes to obtain the required surface smoothness were proposed. In the theoretical design issues, the thesis also described the progress that has been made in Helmholtz equation for an arbitrarily-shaped surface for later numerical analysis.

Whispering gallery mirrors have several advantages over the multilayer mirrors. Its broad band transmission ($\frac{\delta\lambda}{\lambda}$ is $\approx 30\%$ - the peak value of the reflectivity drops by a factor of $\frac{1}{2}$ - in better cases, as in Rh. $\approx 8\%$ in worse cases, as in La shown in Figure I.4, versus $\approx 3\%$ to 4% for multilayer mirrors) and its focusing power make it a superior soft x-ray optics design.

We first examine the literature on the analysis of the whispering gallery modes. The

first analysis was accomplished by Lord Rayleigh for a perfectly conducting cylindrical surface. Wasylkiwskyj and Ishida & Felsen have used several representations (whispering gallery modes plus continuous spectrum intergral, geometrical rays, geometrical rays plus whispering gallery modes) to study the radiation on and within a cylindrical surface. At the end of this literature review, we sketch out our approach to analyze Helmholtz equation for an arbitrarily shaped surface.

We then examine the practical aspects in designing whispering gallery mirrors. The shape of the mirror, on the first order, is independent of the size of the mirror. This allows us designing the sahpe to adapt the focusing design needs. The size of the critical angle is the size of the light's incident angle and the angle that mirror turns. Skin depths, which is crucial in determining the thickness of the coating to be put on the surface of the mirror, are given for a few elements at 200 angstroms. Moreover, we study the scattering loss due to surface roughness. The requirement for the surface irregularities' height is roughly 10 angstroms for a correlation radius of 2 μ and an incoming light of 200 angstroms, to avoid scattering loss. The equations described in the section apply to other wavelengths incident on a bent surface. In the fourth section, we described the Kramers- Kronig relation, which has been the basis of our code for calculating optical constants of interested materials. The phenomenon of Cooper Minimum is described briefly. It serves as the main criterion in our selection of materials for coating.

To build a whispering gallery mirror, we describe the issues that are involved in cutting the surface, selecting the substrate, and polishing the surface. Perkin-Elmers' X-Ray Telescope and Zeiss' ROSAT, our counterparts, have been able to polish the surface irregularities to a height less than 30 angstroms rms or 2 angstroms by Zeiss. Locally, we have found Diamond Electrooptics that can polish metal to a roughness of 15 angstroms rms

and General Optics that can polsih glass to a roughness of 5 angstroms rms.

The following issues still need to be studied and examined for whispering gallery mirror designs. First, the design of a coupler to direct light out of the mirror. Several schemes have been proposed inour group. However much work and research still need to be carried out in this area.

Second, the study of the interaction of the soft x-rays with whispering gallery mirrors. When the soft x-ray plasma hits the surface, the plasma is mostly likely to splatter in all directions. We need to understand this interaction better.

The size of the critical angles at soft x-rays regime places stringent requirement on the alignment of the source and the mirrors. Designs have been studied in our group.

We will pursue the Helmholtz equation analysis for an arbitrarily shaped surface. The outline has been given.

Coding and debuggin work is still needed in caculating the optical constants using Kramers-Kronig.

Appendix A

A DERIVATION OF THE HUYGEN'S PRINCIPLE

The divergence's theorem states:[7,8]

$$\int_v \nabla \cdot \mathbf{A} dx^3 = \oint_s \mathbf{A} \cdot \mathbf{n} dx^2 \qquad (A.1)$$

The vector $\mathbf{A}$, can be formed from two scalar potentials ϕ and ψ by $\phi\nabla\psi$ or $\psi\nabla\phi$.

Let $\mathbf{A}$ first be $\phi\nabla\psi$,

$$\nabla \cdot (\phi\nabla\psi) = (\nabla\psi \cdot \nabla\phi) + \phi\nabla\psi \qquad (A.2a)$$

$$\phi\nabla\psi \cdot \mathbf{n} = \phi\frac{\partial\phi}{\partial n} \qquad (A.2b)$$

(A.1) becomes

$$\int_v (\nabla\psi \cdot \nabla\phi + \phi\nabla^2\phi) dx^3 = \oint_s \phi\frac{\partial\psi}{\partial n} dx^2 \qquad (A.3)$$

We can obtain a similar equation for $\mathbf{A} = \phi\nabla\psi$

$$\int_v (\nabla\phi \cdot \nabla\psi + \psi\nabla^2\phi) dx^3 = \oint_s \psi\frac{\partial\phi}{\partial n} dx^2 \qquad (A.4)$$

Subtracting (4) from (3), we obtain the general equation

$$\int_v (\phi\nabla^2\psi - \psi\nabla^2\phi) dx^3 = \oint_s (\phi\frac{\partial\psi}{\partial n} - \psi\frac{\partial\phi}{\partial n}) dx^2 \qquad (A.5)$$

ϕ is often used to represent the field potential while ψ its Green's function.

If we allow ψ be the scalar wave function $\psi(r,\mathbf{t})$ (with a harmonic time dependence $e^{i\omega t}$), the field ψ satisfies the Helmholtz wave equation,

$$(\nabla^2 + k^2)\psi(x) = 0 \qquad (A.6a)$$

Moreover, if we allow ϕ be the Green's function that satisfies the above Helmholtz equation, so that

$$(\nabla^2 + k^2)G(\mathbf{x},\mathbf{x}') = -\delta(\mathbf{x},\mathbf{x}') \qquad (A.6b)$$

Since our observation point lies within the surface, equation (A.5) becomes

$$\psi(\mathbf{x}) = \oint_s [\psi(\mathbf{x}',\mathbf{n}') \cdot \nabla' \mathbf{G}(\mathbf{x},\mathbf{x}') - \mathbf{G}(\mathbf{x},\mathbf{x}')\mathbf{n}' \cdot \nabla'\psi(\mathbf{x}')]\mathbf{da}' \qquad (A.7)$$

To reach a vectorial representation for $\mathbf{E}(\mathbf{x})$, we let $\psi(\mathbf{x})$ be one of the rectangular component of the field:

$$\mathbf{E}(\mathbf{x}) = \oint_s [\mathbf{E}(\mathbf{n}') \cdot \nabla' G - G(\mathbf{n}' \cdot \nabla')\mathbf{E}]da' \qquad (A.8)$$

This is called the Kirchoff's expansion of the Green's function. (It is also known as the Huygen's principle.)

Appendix B

EIGENFUNCTION EXPANSIONS OF THE GREEN'S FUNCTION

Since the source rays are composed of a number of modes, we need to use the eigenfunction expansions of the Green's function to describe the rays.

If the Green's function is composed of a set of eigenfunctions[8] $\psi_m(\mathbf{r})$.

$$G_k(\mathbf{r}|\mathbf{r}_0) = \sum_n A_m \psi_m(\mathbf{r}) \tag{B.1}$$

where $G_k(\mathbf{r}|\mathbf{r}_0)$ is a Green's function that has its observation point at $\mathbf{r}_0$.

The eigenfunctions $\psi_m(\mathbf{r})$ have an orthonormal set, such that

$$\int \psi_m \psi_n dV = \delta_{nm} \tag{B.2}$$

Green's function satisfies the wave equation,

$$\nabla^2 G_k + k^2 G_k = -4\pi\delta(\mathbf{r} - \mathbf{r}_0) \tag{B.3}$$

The ∇^2 operator introduces $-k_m^2$ factor; consequently,

$$\sum_n (k^2 - k_m^2) A_m \psi_m(\mathbf{r}) = -4\pi\delta(\mathbf{r} - \mathbf{r}_0) \tag{B.4}$$

By multiplying this equation by its orthonormal set and integrating it over the volume, we pick out each A_n

$$A_n = \frac{4\pi\psi_n(\mathbf{r}_0)}{k_n^2 - k^2} \tag{B.5}$$

The eigenfunction expansion of the Green's function is, therefore,

$$G_k(\mathbf{r}|\mathbf{r}_0) = \sum_n \frac{4\pi\psi_n(\mathbf{r}_0)\psi_n(\mathbf{r})}{k_n^2 - k^2} \qquad (B.6)$$

Appendix C

C. LORD RAYLEIGH'S FORMULATION FOR LOSSY MEDIUM

For a lossy medium, we need to construct a field solution outside the boundary surface and match the boundary conditions at the surface. Since we are outside the surface, we do not need to worry about having singularity occur at the origin. Therefore,

$$w_n^{out} = BY_n(hr)e^{ikat}\cos n\theta \qquad (C.1)$$

where $Y_n(kr)$ is the general solution and the time dependence is decoupled from its angular dependence. We expand $Y_n(kr)$ into its integral expression:

$$Y_n(hr) = \frac{J_{-n}(hr) - e^{in\pi}J_n(hr)}{\sin(n\pi)} \qquad (C.2)$$

$$Y_n(hr) = \frac{1}{\pi}\int_0^\infty e^{n\theta - z\sinh\theta}d\theta + \frac{\cos n\pi}{\pi}\int_0^\infty e^{-n\theta - z\sinh\theta}d\theta$$

$$-\frac{1}{\pi}\int_0^\pi \sin(z\sin\theta - n\theta) - \frac{i}{\pi}\int_0^\pi \cos(z\sin\theta - n\theta)\,d\theta \qquad (C.3)$$

For $n \gg kr$, the significant terms of the integral are the first and the last terms. Setting $z = n\cosh\beta$,

$$Y_n(hr) = \left(\frac{\coth\beta}{2n\pi}\right)^{1/2}\left[2e^{-t} - ie^{t}\right] \tag{C.4}$$

$$Y_n'(hr) = -\left[\frac{\sinh\beta\cosh\beta}{2n\pi}\right]^{-1/2}\left\{2e^{-t} + ie^{t}\right\} \tag{C.5}$$

where

$$t = n(\tanh\beta - \beta) \tag{C.6}$$

The field inside still depends solely on $J_n(kr)$. Where $k/h = \mu$, the refractive index with respect to the field outside. We need to consider the case where $\mu > 1$, so that we can have total reflection.

$$w_n^{in} = AJ_n(kr)e^{iakt}\cos n\theta \tag{C.7}$$

The force must be continuous across the boundary. Let ρ and σ be the densities inside and outside the surface respectively:

$$B_\rho Y_n(ha) = A\sigma J_n(ka) \tag{C.8}$$

The normal motion is continuous across the boundary:

$$AkJ_n'(ka) = BhY_n'(ha) \tag{C.9}$$

Let

$$\frac{Y_n'(ha)}{Y_n(ha)} = \sinh\beta \tag{C.10}$$

From the previous approximation for $n \gg z$, (C.4) and (C.5),

$$\frac{J_n'(ka)}{J_n(ka)} = -\frac{k\rho}{\sigma h} \tag{C.11}$$

$$\frac{Y_n'(ha)}{Y_n(ha)} = -\sinh\beta\frac{2e^{-t} + ie^{t}}{e^{-t} - ie^{t}} = -\sinh\beta(1 + ie^{-2t}) \tag{C.12}$$

Letting $x' = x/\mu$ and $y' = y/\mu$,

$$\frac{J_n'}{J_n(x+iy)} = \frac{J_n'(x)}{J_n(x)}\left\{1 - iy\frac{J_n'(x)}{J_n(x)}\right\} \tag{C.13}$$

we obtain,

$$\frac{Y_n'(x'+iy')}{Y_n x'+iy')} = -\sin h\beta\left\{1 + ie^{2t} + iy'\left(-\frac{\cos h\beta}{n} + \sin h^2\beta\frac{Y_n}{Y_n'} - \frac{Y_n'}{Y_n}\right)\right\} \tag{C.14}$$

Adjusting (C.13) by a constant $\frac{k\rho}{\sigma h}$, the first part in the y' terms becomes 0 when n is very big, while the other two terms cancel each other. We arrive at the result,

$$y = \frac{\sigma k}{\rho h}\frac{e^{2t}}{\sinh\beta} = \frac{\mu\sigma}{\rho}e^{\frac{-2n(\beta-\tanh\beta)}{\sinh\beta}} \tag{C.15}$$

β's real part is n and its imaginary part y. We substitute (C.15) for the time dependent term and get

$$ikat = \frac{ikRat}{\mu} = \frac{int}{\mu R}\left\{1 + \frac{1}{n}i\frac{\sigma k}{\rho}e^{\frac{-2n(\beta-\tanh\beta)}{\sinh\beta}}\right\} hspace2in \tag{C.16}$$

If (C.15) is small, the decrease in magnitude for a wave traveled around one circle can be approximated by

$$Transmission = 1 - \frac{2\pi\mu\sigma}{n\rho}e^{\frac{-2n(\beta-\tanh\beta)}{\sinh\beta}} \tag{C.17}$$

If n is big, the damping is not significant. Moreover, the less curved the surface is, the smaller μ needs to be. Therefore, for a lossy medium, the whispering gallery effect may still persist given that the frequency of the waves is high enough.

Appendix D

Wasylkiwskyj's Formulation

1. The Whispering Gallery Modes and the Continuous Spectrum Integral Representation

The Green's function's angular dependence assumes the form:

$$g_\phi(\phi|\phi_0;\nu) = \frac{\exp(i\nu|\phi-\phi_0|)}{-2i\nu} \qquad (D.1)$$

where ϕ_0 denotes the angle at which the source point is located and ν is the propagation constant of the waves.

The Green's function can be expanded into a set of eigenfunctions:

$$G(\bar{r}|\bar{r}_0) = \sum_\nu g_\phi(\phi|\phi_0;\nu)\psi_\nu(r)\psi_\nu(r_0) \qquad (D.2)$$

(D.2) satisfies the wave equation for a cylindrical surface:

$$\left(\frac{1}{r}\frac{\partial}{\partial r}r\frac{\partial}{\partial r} + \frac{1}{r^2}\frac{\partial^2}{\partial\phi^2} + k^2\right) G(\bar{r}|\bar{r}_0) = -\frac{\delta(r-r_0)\delta(\phi-\phi_0)}{r_0} \qquad (D.3)$$

The perfectly reflecting surface has the boundary condition,

$$\frac{\partial}{\partial r}G(\bar{r}|\bar{r}_0)\Big|_{r=a} = 0 \qquad (D.4)$$

with a as the radius of the cylinder.

The eigenfunctions in the r domain satisfy the following relationship:

$$r_0\delta(r-r_0)=\sum_{\nu}\psi_\nu(r)\psi_\nu(r_0)=\frac{1}{2\pi i}\oint g_r(r\big|r_0;\mu)d\mu \qquad (D.5)$$

$G(\bar{r},\bar{r}_0)$ as shown by Wasylkiwskyj, has the following Kontorovich-Lebedev integral form:

$$G(\bar{r},\bar{r}_0)=\frac{\pi}{2}\sum_n e^{i\nu n\left|\phi-\phi_0\right|}\frac{\dot{H}^{(1)}_{\nu_n}(ka)}{\frac{\partial}{\partial\nu}\dot{J}_\nu(ka)\Big|_{\nu=\nu_n}}J_{\nu_n}(kr)J_{\nu_n}(kr_0)$$

$$+\frac{1}{16}\int_0^{i\infty}d\nu e^{i\nu\left|\phi-\phi_0\right|}\frac{\sin\nu\pi}{\dot{J}_\nu(ka)\dot{J}_{-\nu}(ka)}W_\nu(r,a)W_\nu(r_0,a) \qquad (D.6)$$

W is the Wronskian of $H^{(2)}_\nu$ and $H^{(1)}_\nu$.

For each ka, there corresponds a finite number of poles. The terms in the series correspond to the contributions of the poles. They represent the whispering gallery modes. The other contributions sum up and comprise a continuous spectrum representation.

(D.6) has the following form if both the observation point and the source point lie on the surface:

$$G(a,\phi,\phi_0)=\frac{i}{ka}\sum_n e^{i\nu n\left|\phi-\phi_0\right|}\frac{J_{\nu n}(ka)}{\frac{\partial}{\partial\nu}\dot{J}_\nu(ka)\Big|_{\nu=\nu_n}}$$

$$+\frac{1}{2\pi ka}\int_0^{i\infty}d\nu e^{i\nu\left|\phi-\phi_0\right|}\left[\frac{J_\nu(ka)}{\dot{J}_\nu(ka)}-\frac{J_{-\nu}(ka)}{\dot{J}_{-\nu}(ka)}\right] \qquad (D.7)$$

Let us examine the behavior of (D.6) for high frequency fields, i.e., when ka is large. When ka is large, the Bessel's function has the following form:

$$J_\nu(ka)\sim\left(\frac{2}{\alpha}\right)^{1/2}\beta^{1/6}Ai\left[-(\beta)^{2/3}\right] \qquad (D.8a)$$

$$J_\nu(ka)\sim\frac{-1}{ka}(2\alpha)^{1/2}\beta^{-1/6}\dot{A}i\left[-(\beta)^{2/3}\right] \qquad (D.8b)$$

After the expansions, we obtain,

$$G(a,\phi,\phi_0)=\frac{i}{ka}\sum_{n=1}^{N}\frac{e^{ika\left|\phi-\phi_0\right|}\sin w_n}{(\pi/2-w_n)\cos w_n}+$$

$$\frac{1}{\pi}\int_0^{\infty} dv e^{-ka\left|\phi-\phi_0\right|\sin hv} + 0\left(\frac{1}{ka}\right) \qquad (D.9)$$

(D.9) describes the field when both the observation point and the source point lie on the surface. The waves described in (D.9) are evanescent relative to the whispering gallery modes. The last term in (D.9) is the spurious effect generated by the absorbing boundary condition. The second to last term in (D.7) is the difference between the zeroth order Neumann and Struve functions. As the observational point approaches the source point, the Neumann function dominates and approaches the real part of the Green's function for an infinite perfectly conducting plane, while the whispering gallery modes converge to the imaginary part of the expression.

2. Geometrical Ray Representation

To establish a geometrical ray representation of the fields, we use a Fourier transform representation of the Green's function:

$$G(\bar{r}|\bar{r}_0) = \frac{1}{2\pi}\int_{-\infty}^{\infty} e^{i\nu|\phi-\phi_0|} g_r(r|r_0;\nu)d\nu \qquad (D.10)$$

The points of observation and source both lie on the surface and that ka is large, we can expand (D.10) asymptotically and obtain:

$$G(a,\phi,\phi_0) \sim -\frac{1}{2\pi}\int_p dw e^{ika|\phi-\phi_0|}\sin w \frac{\beta^{1/3}Ai[(-(\beta)^{2/3}]}{Ai[-(\beta)^{2/3})]} \qquad (D.11)$$

The path of integration is shown in Figure 2. β in (D.11) works for an arbitrary set of complex numbers,

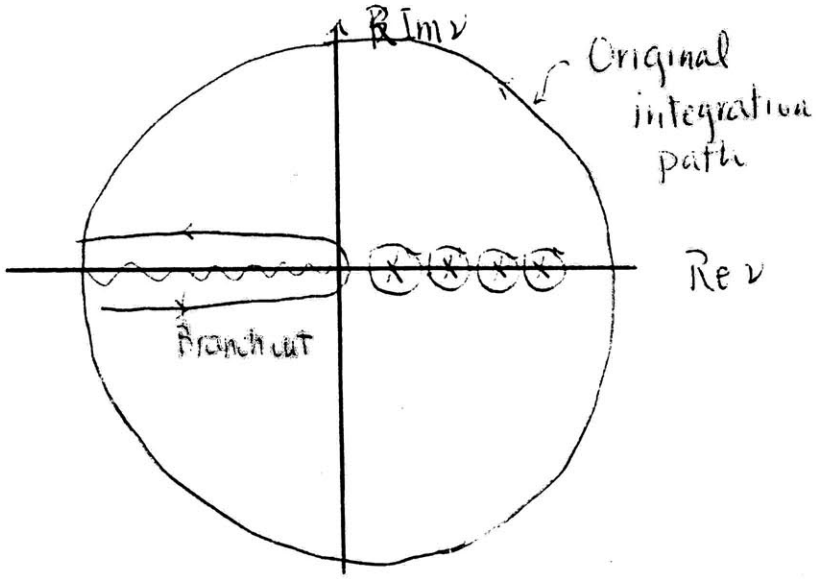

Figure 2

$$\beta = \begin{cases} \frac{3}{2}ka[\cos w - (\frac{\pi}{2} - w)\sin w] & Rew > 0 \qquad (D.12a) \\ \frac{3}{2}ka[\cos w + (\frac{\pi}{2} + w)\sin w] & Rew < 0 \qquad (D.12b) \end{cases}$$

In the previous section, we obtained the whispering gallery mode representation from evaluating the poles in the complex plane. The ray representation, however, is obtained from evaluating the integral through a steepest descent path. We obtain a set of integrals from (D.11) by expressing the denominator in an infinite series l:

$$\frac{1}{Ai[-(\beta)^{2/3}]} = \frac{2}{Ai + iBi}\sum_{l=0}^{\infty}(-1)^l\left(\frac{Ai - iBi}{Ai + Bi}\right)^l \qquad (D.13)$$

The steepest descent paths are paths running through the saddle points:

$$w = \frac{\pi}{2} - \frac{|\phi - \phi_0|}{2l} \qquad l = 1, 2, 3 \qquad (D.14)$$

After evaluating the integrals and some manipulations, we arrive at the ray optics representation of the Green's function,

$$G(a, \phi, \phi_0) \sim \sum_{l=1}^{\infty}(-1)^l e^{i(\pi/2)(l+1)} F_l(a, \phi, \phi_0) \qquad (D.15)$$

where

$$F_l(a, \phi, \phi_0) \sim \sum_{l=1}^{\infty}(-1)^l e^{i(\pi/2)(l+1)} F_l(a, \phi, \phi_0) \qquad (D.16)$$

l is a ray that has been reflected $l - 1$ times.

When l is big, or when we are close to the source point, the amplitude of the ray remains finite. This is somewhat surprising because, from a geometric optics point of view, a large number of caustics would lie close to the source point. The only possible explanation would be for the illuminated region to be of very small value when the observation point approaches the source point. The series itself is divergent as it represents an infinite number of caustic rays.

Wasylkiwkyj also attempted to express the surface field in both rays and an integral expression. As we evaluate the integrals in (D.11), the saddle points become progressively

closer as l increases. The asymptotic Airy integral expressions, which were obtained from the WKB method, break down. The approximations are valid when

$$(\frac{3}{2}kald_l)^{2/3} \equiv (\frac{3}{2}ka)^{2/3}(\frac{|\phi-\phi_0|}{2l} - \sin\frac{|\phi-\phi_0|}{2l})^{2/3} \gg 1 \qquad (D.17)$$

The Green's function becomes,

$$G(a,\phi,\phi_0) \sim \sum_{l-1}^{\infty}(-1)^l e^{i(\pi/2)l+1)l} \qquad (D.18)$$

For large l, (D.18) can be reduced down to

$$I_l \sim \frac{1}{\sqrt{2}}\left(\frac{3}{4}d_l\right)^{1/6} e^{ikalS_l}\left\{\frac{ul+vl}{2kal)^{1/3}}A_2\left[-(\frac{3}{2}kald_l)^{2/3}\right] - i\frac{ul-vl}{(\frac{3}{4}d_l)^{1/3}(2kal)^{2/3}}\dot{A}_2[-(\frac{3}{2}kald_l)^{2/3}]\right\} \qquad (D.19)$$

A large sum of this diverges very quickly because the intensity decays only as $l^{1/3}$.

3. Geometric Optics and the Whispering Gallery Modes Representation

Wasylkiwskyj developed geometric optics and the whispering gallery mode representation by expanding the denominator in (D.11) into the following form:

$$\frac{1}{\dot{A}i} = \frac{2}{\dot{A}_2}\frac{1}{1-y} \equiv \frac{2}{\dot{A}_2}\left(\sum_{l=0}^{L} y^l + \frac{y^{L+1}}{1-y}\right) \qquad (D.20)$$

where

$$y = \frac{\dot{A}_1}{\dot{A}_2} \qquad (D.21)$$

$$\dot{A}_1 = \dot{A}_i - i\dot{B}i \qquad (D.22a)$$

$$\dot{A}_2 = \dot{A}_i + i\dot{B}i \qquad (D.22b)$$

The Green's function has the form

$$G(a,\phi,\phi_0) = \sum_{l=0}^{L} G_l + R_L \qquad (D.23)$$

where

$$G_l = -\frac{1}{\pi}\int_p dw e^{ika\left|\phi-\phi_0\right|\sin w}\beta^{1/3}\frac{Ai}{A_2}y^l \qquad (D.24)$$

and

$$R_L = -\frac{1}{2\pi}\int_p dw e^{ika\left|\phi-\phi_0\right|\sin w}\beta^{1/3}\frac{Ai}{Ai}y^{L+1} \qquad (D.25)$$

The whispering gallery modes are represented by (D.25) which has singularities in its denominator.

L in (D.25) satisfy the condition,

$$(\frac{3}{2}ka)^{2/3}\left[\sin\frac{\left|\phi-\phi_0\right|}{2L} - \frac{\left|\phi-\phi_0\right|}{2L}\cos\frac{\left|\phi-\phi_0\right|}{2L}\right]^{2/3} \gg 1 (D.26)$$

After a number of manipulations, we arrive at the whispering gallery modes and ray optics representation.

$$
\begin{aligned}
G(a,\phi,\phi_0) \;\sim\; & \sum_{l=1}^{L}(-1)^l e^{i(\pi/2)(l+1)} F_l(a,\phi,\phi_0) \\
& + \frac{1}{2}(-1)^{L+1} e^{i(\pi/2)(L+2)} F_{L+1}(a,\phi,\phi_0) \\
& + \frac{i}{ka}\sum_{n=1}^{M} \frac{e^{ika\left|\phi-\phi_0\right|\sin Wn}}{(\pi/2 - W_n)\cos Wn}
\end{aligned}
\qquad (D.27)
$$

where $F_l(a,\phi,\phi_0)$ is given in (D.16).

Appendix E

E. Bahar's Formulation

E. Bahar analyzed the high frequency field on a surface that is of both varying impedance and curvature.[5] This is a more general approach than the one undertaken by Ishihara, Felsen, and Wasylkiwskyj. However, Bahar did not generate numerical results.

Bahar describes a surface of arbitrary curvature and variable impedance by x, y, and z.

The coordinates are defined in the following way: Surfaces on which x are constant are normal to our surface; surfaces on which y are constant enclose the surface ($y > 0$, when y is outside our surface); surfaces on which z are constant are normal to the axis of the cylinder.

The x, y, z coordinates are related to the cylindrical coordinates in the following Jacobians:

$$J_T^{-1} = \begin{vmatrix} \frac{\partial r}{\partial x} & \frac{\partial r}{\partial y} \\ \frac{\partial \phi}{\partial x} & \frac{\partial \phi}{\partial y} \end{vmatrix} = \begin{vmatrix} \frac{dR}{dx} & 1 \\ \frac{1}{R} & 0 \end{vmatrix} \qquad (E.1a)$$

$$J_T = \begin{vmatrix} \frac{\partial x}{\partial r} & \frac{\partial x}{\partial \phi} \\ \frac{\partial y}{\partial r} & \frac{\partial y}{\partial \phi} \end{vmatrix} = \begin{vmatrix} 0 & R \\ 1 & -\frac{RdR}{dx} \end{vmatrix} \qquad (E.1b)$$

The Maxwell's equations in cylindrical coordinates can be made to depend on x and r while eliminating the ϕ dependent component of the magnetic field. We obtain:

$$-\frac{\partial E_z}{\partial x} = i\omega\mu\frac{r}{R}H_r \tag{E.2a}$$

$$-\frac{\partial H_r}{\partial x} = i\omega\epsilon\left[\frac{r}{R}E_z + \frac{1}{k^2}\frac{\partial}{\partial r}\left(\frac{r}{R}\frac{\partial E_z}{\partial r}\right)\right] + \frac{r}{R}J_z \tag{E.2b}$$

where $k = \omega(\mu\epsilon)^{1/2}$ and $J_z = \frac{I\delta(r-r_0)\delta(x-x_0)}{R}$.

For the cylindrical case, where $r = R$, E_z satisfies the following scalar wave equation:

$$\nabla^2 E_z = \frac{1}{r}\frac{\partial}{\partial r}(r\frac{\partial E_z}{\partial r}) + \frac{1}{r^2}\frac{\partial^2 E_z}{\partial \phi^2} + k^2 E_z = i\omega\mu J_z \tag{E.3}$$

E_z can be expanded into the following eigenfunction expressions for zero impedance.

$$E_z(\xi,\phi) = -\frac{\omega\mu\pi I}{4}\sum H^{(2)}_{\nu_n}(\xi_0)H^{(2)}_{\nu_n}(\xi)\times \left(\frac{H^{(1)}_{\nu}(\xi_R)}{\frac{\partial H^{(2)}_{\nu}(\xi_R)}{\partial \nu}}\right)_{\nu_n}\frac{\cos\nu_n(\phi-\phi_0-\pi)}{\sin\nu_n\pi} \tag{E.4}$$

where $H^{(1,2)}_{\nu_n}(\xi)$ are the Hankel functions of the first and second kind and that ξ and ξ_R denote the number of waves in the specified radius.

The electromagnetic fields satifies the impedance boundary condition at $r = R$,

$$\frac{\partial E_z}{\partial(kr)} = \frac{i\eta E_z}{Z_s} \tag{E.5}$$

where η is the intrinsic impedance of the medium.

Each order ν_n of the basis functions satisfy the equation

$$H^{(2)'}_{\nu_n}(\xi_R) - \frac{i\eta}{Z_s}H^{(2)}_{\nu_n}(\xi_R) = 0 \tag{E.6}$$

We can write the azimuthal dependence of (E.4) as a superposition of the forward traveling and backward traveling waves:

$$E_z(\xi,x)=\sum_{n=1}^{\infty}e_n(x)\frac{H_{\xi_n}^{(2)}(\eta)}{N_n}\equiv\sum_n[a_n(x)+b_n(x)]\frac{H_{\nu_n}^{(2)}(\xi)}{N_n} \tag{E.7}$$

$$a_n(\phi)+b_n(\phi)=2i\left(e^{-i\nu_n(\phi-\phi_0)}+e^{-i\nu_n(\phi-\phi_0-2\pi)}\right)\sum_{p=0}^{\infty}e^{-ip\omega\pi\nu_n} \tag{E.8}$$

The electric field amplitude $e_n(x)$ can be expressed to be the transform of the function using the orthogonal properties of the basis functions.

$$e_n(x)=\int_{\xi_R}^{\infty}E_z(\xi,x)\left(\frac{H_{\nu_n}^{(2)}(\xi)}{M_n}\right)\nu_n\frac{\partial\xi}{\xi} \tag{E.9}$$

We can express the magnetic fields in a similar way:

$$H_r(\xi,x)=\sum_{n=1}^{\infty}h_n(x)\frac{Y_n(\xi)H_{\nu_n}^{(2)}(\xi)}{N_n}\equiv\sum_{n=1}^{\infty}[a_n(x)-b_n(x)]\frac{Y_n(\xi)H_{\nu_n}^{(2)}(\xi)}{N_n} \tag{E.10}$$

where

$$h_n(x)=\eta\int_{\xi_R}^{\infty}H_r(\xi,x)H_{\nu_n}^{(2)}\frac{\partial\xi}{M_n} \tag{E.11}$$

The forward traveling waves, as noted before by Lord Rayleigh and others, constitutes not only the direct wave propagating in the positive x direction but also the whispering gallery waves which propagate around the cylinder p times (p is an integer).

For $kR\gg 1$ and for lossy surfaces, we may retain only direct waves:

$$a_n'(x)\approx -J_0\left(\frac{M_n(x_0)}{N_n(x)}M_n(x)N_n(x_0)\right)^{1/2}exp\left(-i\int_{x_0}^{x}\nu_n\frac{du}{R}\right) \tag{E.12}$$

The disappearance of the whispering waves conforms to our intuition because such waves would have been absorbed by the surface before they propagate around again.

After a number of manipulations, we obtain for the amplitudes of the traveling waves:

$$a_n(x) = -\int_0^x \frac{dT_{n_0}}{du} a_0(u) \times exp\left[-\int_u^x \left(\frac{dT_{nn}}{dv}\right) + i\left(\frac{\nu_n}{R}\right) dv\right] du \qquad (E.13)$$

$$b_n(x) = -\int_x^\infty \frac{dT_{n_0}}{du} a_0(u) \times exp\left[-\int_u^x \left(\frac{dT_{nn}}{dv}\right) - i\left(\frac{\nu_n}{R}\right) dv\right] du \qquad (E.14)$$

For $M_n = N_m = 1$,

$$\frac{dT_{nm}}{dx}\Big|_{R=const} = \frac{-i dy_s/dx}{\nu_n - \nu_m} H^{(2)}_{\nu_n}(\xi)\left(\frac{\partial}{\partial \nu}\left[H^{(2)\prime}_{\nu}(\xi_R) - i y_s H^{(2)}_{\nu}(\xi_R)\right]_{nu_n}\right)^{-1}$$

$$= -\frac{d\mu_n/dx}{\nu_n - \nu_m} \frac{H^{(2)}_{\nu_m}(\xi_R)}{H^{(2)}_{\nu_n}(\xi_R)}, \qquad n \neq m \qquad (E.15)$$

$$\frac{dR_{nm}}{dx}\Big|_{R=const} = \frac{\nu_n - \nu_m}{\nu_n + \nu_m} \frac{dT_{nm}}{dx}\Big|_{R=const}, \qquad n \neq m \qquad (E.16)$$

VI. References

I. INTRODUCTION

[1] Vinogradov, A. V., and B. Ya. Zeldovich, "Multilayer mirrors for x-rays and far-ultraviolet radiation," *Opt. Spectrosc.*, v. 42, no. 4, 404.

[2] Vinogradov, A. V., "XUV Cavity and Pumpuing Optics," *J. de Physique*, International Colloqium on X-Ray Laser, October 1986, C6-287.

[3] Lee, Ping, "Application of the WKB Method to X-Ray Diffraction by One Dimensional Periodic Structure," *Optics Communications*, v. 42, no. 3, 195.

[4] Spiller, Eberhard, "Low Loss Reflection Coatings Using Absorbing Materials," *APL*, v. 20, no. 9, 365.

[5] Daneu, V., "Optical Thickness Monitor for Thin Film Deposition," *Applied Optics*, v. 14, no. 4, 962.

[6] Gaponov, S. V., and N. N. Salashchenko, "Multilayer mirrors for x-rays and far-ultraviolet radiation," *Opt. Spectrosc.*, v. 46, no. 8, 1543.

[7] Barbee, Troy W., Jr., "Sputtered Layered Synthetic Microstructure (LSM) Dispersion Elements," *AIP Conference 1975, Boulder, Colorado*, 131.

[8] Vinogradov, A. V., and B. Ya. Zeldovich, "X-ray and far uv multilayer mirrors: principles and possibilities," *Applied Optics*, v. 16, no. 1, 89.

[9] Ceglio, N. M., D. G. Stearns, D. P. Gaines, A.M. Hawryluk, and J. E. Trebes, "Multipass amplification of soft x rays in a laser cavity,"z*Optics Letters*, v. 13, 108.

II. Present Status of Whisper Gallery Mirrors

[1] Lord Rayleigh, "The Problem of the Whispering Gallery", *Philosophical Magazine SG*, Vol. 20, Dec. 1910, 1001.

[2] Lord Rayleigh, "Further Applications of Bessel's Functions of high order to the Whispering Gallery and allied Problems",*Philosophical Magazine*, Vol. 20, 1914, 100.

[3] Wasylkiwskyj, Wasyl, "Diffraction by a Concave Perfectly Conducting Circular Cylinder", *IEEE Transactions on Antennas and Propagation*, Vol. AP-23, No. 4, July 1975, 480.

[4] Ishihara, T. and Felsen, L. B., "High-Frequency Fields Excited by a Line Source Located on a Perfectly Conducting Concave Cylindrical Surface", *IEEE Transactions on Antennas and Propagation*, Vol. AP-26, No.6, November 1978, 757.

[5] Bahar, E., "Diffraction of Electromagnetic Waves by Cylindrical Structures Characterized by Variable Curvature and Surface Impedance", *Journal of Mathematical Physics*, Vol. 12, No. 2, February 1971, 186.

[6] Rayleigh, John William Strutt, *Theory of Sound*. New York, 1945, 395.

[7] Jackson, J. D., *Classical Electrodynamics.* New York. 1975.

[8] Morse, Philip M. and Herman Feshbach, *Methods of Theoretical Physics, Part I..* 1953.

III. Design of Whisper Gallery Mirrors III.A.2 Glancing Angles

[1] Vinogradov, A. V., et. al., "Selection of materials for concentrators designed for optical pumping of ultraviolet and vacuum ultraviolet lasers," *Sov. J. Quant. Elect.*, **16**(12), 1602.

[2] Vinogradov, A. V., and S. I. Sagitov, "New types of mirrors for the soft x-ray range (review)," *Sov. J. Quant. Elect.*, **13**(11), 1439.

[3] Vinogradov, A. V., and I. V. Kozhevnikov, "Properties of x-ray waveguies," *Sov. Phys. Tech. Phys.*, **29**(9), 1023.

[4] Vinogradov, A. V., et. al., "Deflection of a soft x-ray beam by a spherical surface," *Sov. Phys. Doklady*, **32**(1), 64.

[5] Vinogradov, A. V., et. al., "Concave rotating x-ray mirror: I," *Sov. Phys. Tech. Phys.*, **30** (2), 145.

[6] Vinogradov, A. V., et. al., "Diffraction theory for grazing modes in concave mirrors and resonators at x-ray wavelengths: II," *Sov. Phys. Tech. Phy.*, **30** (3), 335.

[7] Vinogradov, A. V., "Optical theorem for scattering with a boundary," *Sov. Phys. Doklady*, **31**(2), 143.

[8] Vinogradov, A. V., "Broad band mirrors for ultraviolet and soft x-ray radiation," *Sov. Phys. Doklady*, **27**(9), 741.

[9] Vinogradov, A. V., "XUV Cavity and Pumpuing Optics," *J. de Physique*, International Colloqium on X-Ray Laser, October 1986, C6-287.

[10] Shen, L. C. and J. A. Kong, *Applied Electromagnetism*, 1987.

[11] Cox, J. Thomas et. al., "Optical properties of evaporated Rhodium films deposited at various substrate temperatures in teh vacuum ultraviolet from 150 to 2000 angstroms, " *J. of Opt. Soc. of America*, v. 61, no. 3, 360.

[12] Juenker, D. W., et. al., "Optical Properties of Some Transition Metals," *J. of Opt. Soc. of America*, v. 58, no. 2, 164.

[13] Rieser, L. M., Jr., "Reflectance of X-Rays from Condensed Metal Films," *J. of Opt. Soc. of America*, v. 47, no. 11, 987.

[14] Weaver, J. H., et. al., "Optical properties of metals, " *Applied Optics*, v. 20, no. 7, 1124.

III.A.3 Perturbation Analysis of Surface Roughness of the Whisper Gallery Mirrors

[1] Vinogradov, A. V., "Phenomenon of total external reflectio of x rays," *Sov. Phys. JETP*, **62**(6), 1225.

III.A.4 Kramers-Kronig Analysis

[1] Jackson, J. D., *Classical Electrodynamics.* New York. 1975.

[2] Henke, B. L., et. al., "Low Energy X-Ray Interaction Coefficients: Photoabsorption, Scattering, and Reflection," *Atomic Data and Nuclear Data Tables*, v. 27, no. 1, 1.

[3] Barfield, W. D., and W. F. Huebner, "On the Calculation of Scattering Cross Sections from Absorption Cross Section," *J. Quant. Spectrosc. Radiat. Transfer*, v. 16, 27.

[4] Fano, U. and J. W. Cooper, "Spectral Distribution of Atomic Oscillator Strengths," *Review of Modern Physics*, v. 40, no. 3, 441.

[5] Manson, Steven T. and John W. Cooper, "Photoionization in the Soft X-Ray Range: Z-dependence in a Central-Potential Model," *Phys. Rev.*, v. 165, no. 1, 126.

[6] Cooper, J. W., "Interaction of Maxima in the Absorption of Soft X-Rays," *Phys. Rev. Lett.*, v. 13, no. 25, 762.

[7] Cooper, J. W., "Photoionization from Outer Atomic Subshells, A Model Study," *Phys. Rev.*, v. 128, no. 2, 681.

III.B Theoretical Designs

[1] Jackson, J. D., *Classical Electrodynamics.* New York. 1975.

[2] Morse, Philip M. and Herman Feshbach, *Methods of Theoretical Physics, Part I.*. 1953.

[3] Prudnikov, A. P., Yu. A. Brychkov, and O. I. Marichev, *Integrals and Series*, 1983.

IV. Implementation Issues

[1] MIT Chemistry Machine Shop, personal communications.

[2] *Metal Finishing, Guidebook Driectory 1988*, 18.

[3] DeCew, Alan, personal communications.

IV.A Construction of the Whisper Gallery Mirrors Locally

[1] Young, Peter S., "Fabrication of the high resolution mirror assembly for the HEAO-2 x-ray telescope," SPIE, v. 184, 131.

[2] Beckstette K., "Aspects of Manufacturing Grazing Incidence X-Ray Mirrors," SPIE, v. 645, 58.

[3] DeCew, Alan, personal communications.

[4] General Optics, personal communications.

IV.B Surface Quality

[1] Young, Peter S., "Fabrication of the high resolution mirror assembly for the HEAO-2 x-ray telescope," SPIE, v. 184, 131.

[2] Bennett, Jean. M., "Measurement of rms roughness, autocovariance function and other statistical properties of optical surfaces using a FECO scanning interferometer," *Appl. Optics*, v. 15, no. 11, 2705.

[3] DeCew, Alan, personal communications.

[4] Lohmann, A. W., and D. P. Paris, "Binary Fraunhofer Holograms Generated by Computer," *Appl. Optics*, v. 6, no. 10, 1739.

[5] Lee, Wai Hon, "Sampled Fourier Transform Hologram Generated by Computer," *Appl. Optics*, v. 9, no. 3, 639.

[6] Smith, David C., "Testing diamond turned aspheric optics using computer-generated hologram (CGH) interferometry," SPIE, v. 306, p. 112.

[7] Emmel, Peter M. and Kang M. Leung, "A New Instrument for Routine Optical Testing of General Aspherics," SPIE, v. 171, 93.

[8] Leung, K. M., et. al, "Using e-beam written computer-generated holograms to test deep aspheric wavefronts," SPIE, v. 306, 161.

Appendices

[1] Lord Rayleigh, "The Problem of the Whispering Gallery", *Philosophical Magazine SG*, Vol. 20, Dec. 1910, 1001.

[2] Lord Rayleigh, "Further Applications of Bessel's Functions of high order to the Whispering Gallery and allied Problems",*Philosophical Magazine*, Vol. 20, 1914, 100.

[3] Wasylkiwskyj, Wasyl, "Diffraction by a Concave Perfectly Conducting Circular Cylinder", *IEEE Transactions on Antennas and Propagation*, Vol. AP-23, No. 4, July 1975, 480.

[4] Ishihara, T. and Felsen, L. B., "High-Frequency Fields Excited by a Line Source Located on a Perfectly Conducting Concave Cylindrical Surface", *IEEE Transactions on Antennas and Propagation*, Vol. AP-26, No.6, November 1978, 757.

[5] Bahar, E., "Diffraction of Electromagnetic Waves by Cylindrical Structures Characterized by Variable Curvature and Surface Impedance", *Journal of Mathematical Physics*, Vol. 12, No. 2, February 1971, 186.

[6] Rayleigh, John William Strutt, *Theory of Sound.* New York, 1945, 395.

[7] Jackson, J. D., *Classical Electrodynamics.* New York. 1975.

[8] Morse, Philip M. and Herman Feshbach, *Methods of Theoretical Physics, Part I..* 1953.